

# The relationship between angular velocity and power efficiency of a helicopter in hover

**Research Question:** *What is the relationship between angular velocity and power efficiency of a twin bladed, single rotor helicopter system in hover?*

**Word Count:** 3998

**Subject:** Physics

# Contents

<b>1</b>	<b>Introduction</b>	<b>3</b>
<b>2</b>	<b>Background Information</b>	<b>4</b>
2.1	Induced velocity and thrust . . . . .	5
2.2	Power and power efficiency . . . . .	7
<b>3</b>	<b>Extending Power Efficiency</b>	<b>8</b>
<b>4</b>	<b>Slipstream Correction for Pitch Angle</b>	<b>9</b>
<b>5</b>	<b>Determining Thrust Coefficient</b>	<b>11</b>
5.1	Determining inflow angle of attack . . . . .	12
5.2	Determining lift-curve gradient . . . . .	14
5.3	Determining thrust coefficient . . . . .	18
<b>6</b>	<b>Determining Power Coefficient</b>	<b>19</b>
6.1	Determining drag coefficient . . . . .	21
6.2	Determining power coefficient . . . . .	21
<b>7</b>	<b>Determining Experimental Power Coefficient</b>	<b>24</b>
7.1	Experimental Setup . . . . .	24
7.2	Experiment procedure . . . . .	24
7.3	Theoretical vs experimental power coefficient . . . . .	25
<b>8</b>	<b>Determining Power Efficiency</b>	<b>27</b>
<b>9</b>	<b>Evaluation and Conclusion</b>	<b>28</b>
<b>10</b>	<b>Works Cited</b>	<b>30</b>
<b>11</b>	<b>Appendix</b>	<b>31</b>
11.1	Appendix 1: Simplifying Reynolds Number . . . . .	31
11.2	Appendix 2: Conversion between Angular Velocity and Reynolds Number . . .	32

11.3 Appendix 3: Determination of Lift-curve Gradient . . . . .	33
11.4 Appendix 4: Determination of Thrust Coefficient . . . . .	34
11.5 Appendix 5: Determination of Drag Coefficient . . . . .	35
11.6 Appendix 6: Determination of Power Coefficient . . . . .	36
11.7 Appendix 7: Raw Experimental Data . . . . .	37
11.8 Appendix 8: Determination of Power Efficiency . . . . .	44
11.9 Appendix 9: Arduino Code for Modulating Motor RPM . . . . .	45

# 1 Introduction

Helicopters are used for their ability to take off and land vertically, qualifying them for a host of tasks, namely: tourism, aerial observation and medical transportation (“Helicopter Career Info”, 2017). An intriguing physics phenomenon of a helicopter, is its potential to hover. A twin bladed single rotor helicopter, consumes 60 - 85% more power to hover than with forward flight, making the manoeuvre inefficient (Lombardi, 2017). A vast amount of literature has been published for optimising blade shape and fuselage weight, in order to enhance efficiency. However, the role of a rotors angular velocity has never been addressed.

Hence, this essay attempts to answer the question “What is the relationship between angular velocity and power efficiency of a twin bladed single rotor helicopter system, in hover?” The essay seeks to correct Froude’s momentum and Drzewiecki’s blade element theory, to obtain a theoretical model for power efficiency in terms of angular velocity. In order to test validity of the theoretical model, an experiment is devised to evaluate the correlation between theoretical and empirical power data.

Firstly, the essay delves into Froude’s model and realises the necessity of thrust and power coefficient in expressing power efficiency. To accommodate NACA 0015 aerofoil geometry used within the experiment, coefficients are corrected by integrating small blade elements along the blade using Drzewiecki’s model. Thereafter, a dependence between air resistance and thrust coefficient is established and incorporated using XFOIL simulations. The simulation allows to compare thrust and power coefficient against angular velocity with industrial specifications, providing insights into hypothetically inefficient, ideal and efficient ranges for power in terms of angular velocity. Correspondingly, the absolute uncertainty for coefficients are found to be substantially large; losing confidence with the theoretical model. Hence, to affirm if the investigation is concurrent with empirical data, an experiment is devised to simulate a helicopter rotor; obtaining data for power coefficient. The empirical and theoretical power coefficient establish a strong correlation, which implied the uncertainties accumulated as a consequence of extensive mathematical calculations. Ultimately, the calculated coefficients were substituted in the model, yielding a clear relationship between power efficiency and angular velocity.

This research question is worthy of investigation, as it advances the understanding and provides impetus to the research in power performance of aerial craft’s. Commercially, we

observe the demand of various clients including: airlines and hobbyists who desire to minimise battery drain time and maximise usage, leading to the central question of power efficiency.

## 2 Background Information

Power dissipated is product of force imparted on air and mean air velocity. Therefore, in order to establish a theoretical model for power efficiency, we must inspect airflow velocity and the different forces in a rotor system.

A hovering helicopter is considered at rest, since the body has zero acceleration and so zero net-force. The airscrew of twin bladed single rotor helicopter rotates around central z-axis, propelling air in a downwards vortex known as the slipstream, figure 1. The slipstream is governed by an inverse relationship termed the venturi effect, where the decreasing cross-sectional area ( $A$ ), increases air velocity ( $\bar{v}$ ) (Halliday et al., 2014). In the early 20<sup>th</sup> century, William Froude combined venturi effect with Bernoulli's principle; formulating an equation for the axial force (z-plane) lifting a helicopter - thrust ( $T$ ).

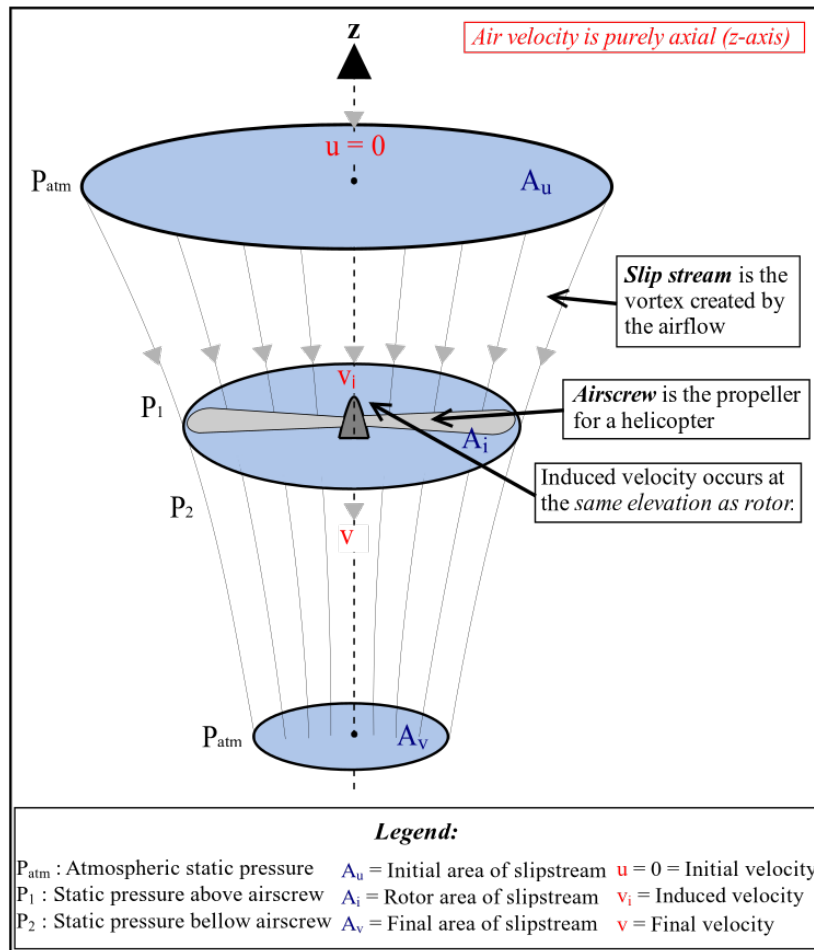


Figure 1: A slipstream for twin bladed single rotor helicopter.

According to Bernoulli's principle, the rotor system experiences dynamic pressure ( $P_d$ ) inside and static pressure ( $P_s$ ) outside the slipstream boundary, which always adds to a constant (1). The dynamic pressure, characteristically exhibits proportionality with airflow velocity:  $P_d \propto \bar{v}$  (Zhao et al., 2019). We assume air density is  $\rho = 1.23kgm^{-3}$  for simplicity, although the value varies with elevation.

$$\Sigma P = P_s + P_d = \text{constant}$$

$$\Sigma P = P_s + \frac{1}{2}\rho\bar{v}^2 = \text{constant} \quad (1)$$

The airflow velocity increases along slipstream from initial velocity ( $u = 0ms^{-1}$ ) above to final velocity ( $v$ ) below the airscrew, proportionally increasing dynamic pressure. Therefore, the cross-sectional area decreases from  $A_u$  above to  $A_v$  below the airscrew by the venturi effect, proportionally decreasing static pressure from  $P_1$  to  $P_2$  respectively; preserving the constant relationship in (1).

$$\text{Above airscrew: } \Sigma P = P_1 + \frac{1}{2}\rho u^2$$

$$\text{Bellow airscrew: } \Sigma P = P_2 + \frac{1}{2}\rho v^2$$

$$P_1 + \frac{1}{2}\rho u^2 = P_2 + \frac{1}{2}\rho v^2$$

Rearranging the equation to find pressure differential experienced by airscrew.

$$P_1 - P_2 = \frac{1}{2}\rho(u^2 - v^2)$$

$$\text{Dynamic pressure differential: } \Delta P_d = P_2 - P_1 = \frac{1}{2}\rho v^2 \quad (\text{Since, } u = 0ms^{-1})$$

## 2.1 Induced velocity and thrust

Froude argued, since pressure is quotient of net-force and cross-sectional area, the greater dynamic pressure beneath the blade causes an upwards directed net-force, figure 2. This net-force is termed thrust, acting orthogonal to airflow on the airscrew (2) (Venkatesan, 2012).

The airscrew area is assumed to be circular where blade's radius is  $R$ , denoted by  $A_i = \pi R^2$ .

$$\Sigma \text{Force}_{net} = P_d(A_i)$$

$$T = \frac{1}{2} A_i \rho v^2$$

$$T = \frac{1}{2} \rho \pi R^2 v^2 \quad (2)$$

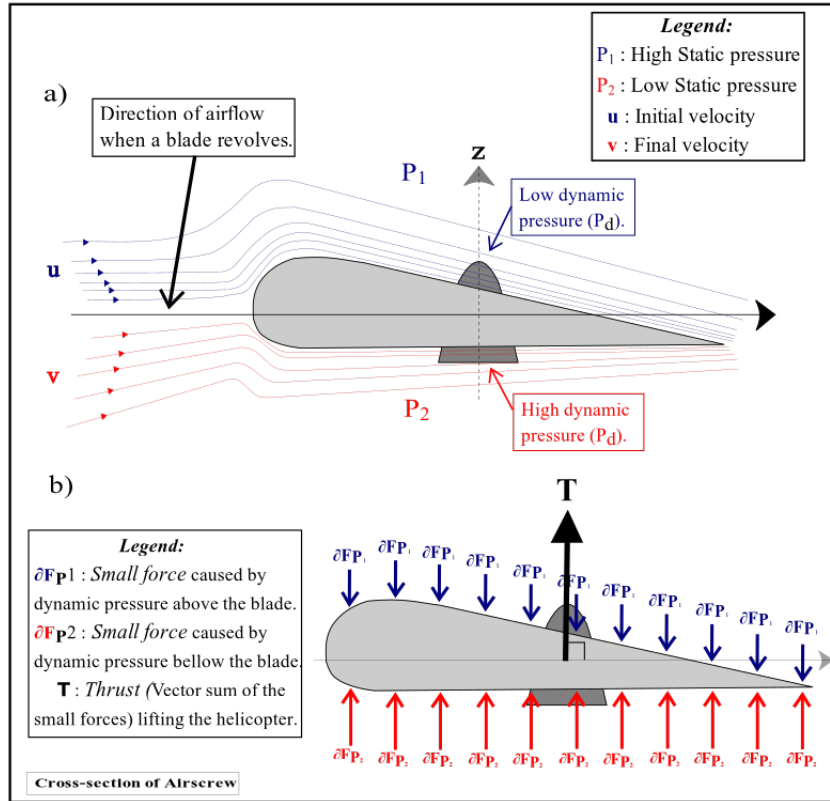


**Figure 2:** Froude uses Bernoulli's principle and properties of venturi effect to model thrust ( $T$ ) in a rotor system.

Conversely, Froude proposed an alternative argument where air particles are the frame of reference. Air particles have negligible mass, requiring mass flow rate ( $\dot{m}$ ) defined as the fluid mass passing airscrew per unit time. Mass can also be considered as volumetric density ( $m = V\rho$ ), where velocity of air positioned at rotor is known as induced velocity ( $v_i$ ).

$$\dot{m} = \frac{\Delta m}{\Delta t}$$

$$\dot{m} = \frac{V\rho}{t} \implies \rho A_i v_i$$

Elastic collision occurs between air particles and airscrew for conserving momentum in sys-

tem, producing an equal and opposite axial thrust force (Gessow & Myers, 1985). Substituting  $\dot{m}$  in Newton's second law, we obtain thrust (3). We assume ideal gas properties are preserved in such high pressure situations for simplicity.

$$F = ma \implies \dot{m}(\Delta\bar{v})$$

$$T = \rho A_i v_i (v - u)$$

$$T = \rho \pi R^2 v_i v \quad (\text{Since, } u=0\text{ms}^{-1}) \quad (3)$$

Realising (2) and (3) model thrust and also incorporate similar variables except for velocity, equating the two expressions yields an important velocity identity (4).

$$T = \rho \pi R^2 v_i v = \frac{1}{2} \rho \pi R^2 v^2$$

$$2v_i = v \quad (4)$$

Thereby, substituting velocity identity within (2) and (3) we are able to derive unified thrust equation (5). Moreover, by isolating induced velocity we determine an equation for velocity at the airscrew (6). This model for force and velocity is Froude's momentum theory (Gessow & Myers, 1985).

$$T = \rho \pi R^2 v_i (2v_i) = \frac{1}{2} \rho \pi R^2 (2v_i)^2$$

$$T = 2\rho \pi R^2 v_i^2 \quad (5)$$

$$v_i = \sqrt{\frac{T}{2\rho \pi R^2}} \quad (6)$$

## 2.2 Power and power efficiency

Recalling from earlier, power ( $\bar{P}$ ) can now be defined as the product of axial thrust force orthogonal to airflow and induced air velocity shown in (7).

$$\bar{P} = Fv \implies T v_i \quad (7)$$

Power efficiency is the ratio between useful and total power, expressed in percentage. In

fluid mechanics, useful power is represented by (7), as here the fluid behaves in an ideal system without viscosity. Viscosity measures a fluids resistance to deformation (Adminstration, 2020). Total power refers to power measured experimentally ( $\bar{P}_{exp}$ ), where aerodynamic losses due to resistive forces are considered. Hence, expanding for power efficiency yields (8):

$$\eta = \frac{\text{Useful Power}}{\text{Total Power}} \times 100 \implies \frac{Tv_i}{P_{exp}} \times 100 \quad (8)$$

The exploration in deriving power efficiency has laid the foundation for this essay. This foundation allows incorporating the important concept of angular velocity.

### 3 Extending Power Efficiency

Investigations in fluid mechanical systems incorporate coefficients, as they allow simplifying power performance equations (Gessow & Myers, 1985). The thrust coefficient ( $c_T$ ) recognises ratio between total thrust produced and cross-sectional area (9). Similarly, power coefficient recognises ratio between power required and cross-sectional area (9). These coefficients recognise blade velocity in circular motion,  $v_{blade} = \omega R$ , where  $\omega$  represents the blade's angular velocity. Also notice, these equations are non-dimensional thus, have no unit.

$$\text{Thrust coefficient: } T = c_T \rho \pi R^2 (\omega R)^2 \quad \text{Power coefficient: } \bar{P} = c_P \rho \pi R^2 (\omega R)^3$$

$$c_T = \frac{T}{\rho \pi R^2 (\omega R)^2} \quad c_P = \frac{\bar{P}}{\rho \pi R^2 (\omega R)^3} \quad (9)$$

In order to substitute the coefficients for power efficiency, we first require to express induced velocity in terms of the coefficients. Therefore, induced velocity from (6) simplifies to (10).

$$v_i = \sqrt{\frac{T}{2\rho\pi R^2}} = \sqrt{\frac{c_T \rho \pi R^2 (\omega R)^2}{2\rho\pi R^2}}$$

$$v_i = \omega R \sqrt{\frac{c_T}{2}} \quad (10)$$

Substituting induced velocity (10), thrust and power coefficient in (8), we obtain a simplified

form of power efficiency (11).

$$\eta = \sqrt{\frac{c_T^3}{2c_P^2}} \times 100 = 70.7 \times \frac{c_T^{\frac{3}{2}}}{c_P} \quad (11)$$

The sections hereafter are based on calculating thrust and power coefficients to determine a relationship between power efficiency and angular velocity ( $\omega$ ).

## 4 Slipstream Correction for Pitch Angle

Pitch angle/ pitch ( $\theta$ ) refers to the angle a blade makes with the horizontal (x-axis). Empirical analysis confirms, thrust cannot be produced without pitch (Venkatesan, 2012). Unified thrust in (5) assumes a zero pitch system hence, it fails to satisfy properties changing with pitch. These properties are illustrated in figure 3 and table 1.

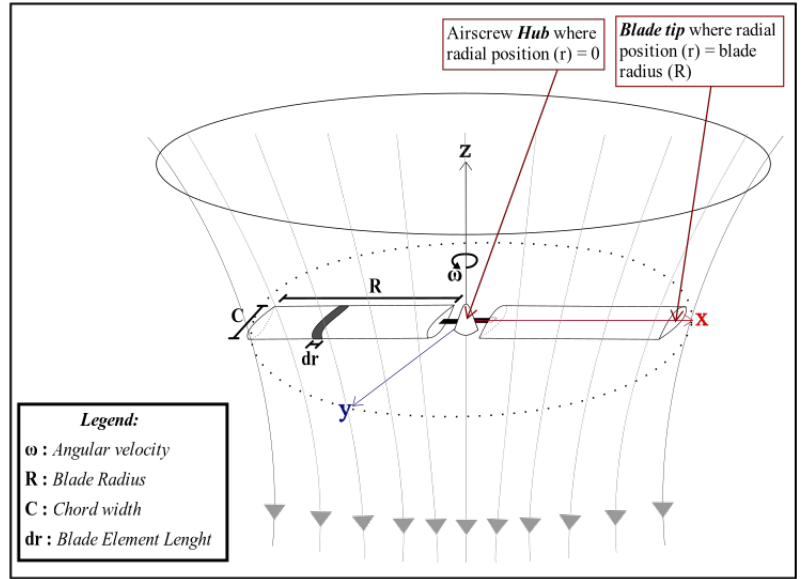


**Figure 3:** A modified approach to the slipstream model.

Properties changed	Description
Angular velocity ( $\omega$ )	A blade rotating through air, is similar to air flowing across a stationary blade with angular velocity ( $\omega$ ) and tangential velocity ( $\omega r$ ), depending on the radial position of blade ( $r$ ).
Inflow velocity ( $v_i$ and $\omega r$ )	Along with induced velocity (z-plane), air also has tangential velocity: $\omega r$ (x-y plane). The vector sum of velocities is resultant velocity, $v_R$ (12).

**Table 1:** Properties that change in a system when implementing a blade pitch angle

$$v_R = \sqrt{v_i^2 + (\omega r)^2} \quad (12)$$

Due to these properties, pitch comprises of inflow angle of attack (Inflow AoA ( $\phi$ )) and angle of attack (AoA ( $\alpha$ )), demonstrated in figure 4 and (13). The inequality  $\theta > \phi$  and  $\theta > \alpha$

holds true, hence by small angle approximation the quotient of induced and tangential velocity;  $\tan \phi$  approximately equal  $\phi$  (14). As inflow AoA is small, so is induced velocity and therefore resultant velocity in (12) is best approximated by tangential velocity (15).

$$\theta = \phi + \alpha \quad (13)$$

$$\tan \phi = \frac{v_i}{\omega r} \approx \phi \quad (14)$$

$$v_R \approx \omega r \quad (15)$$

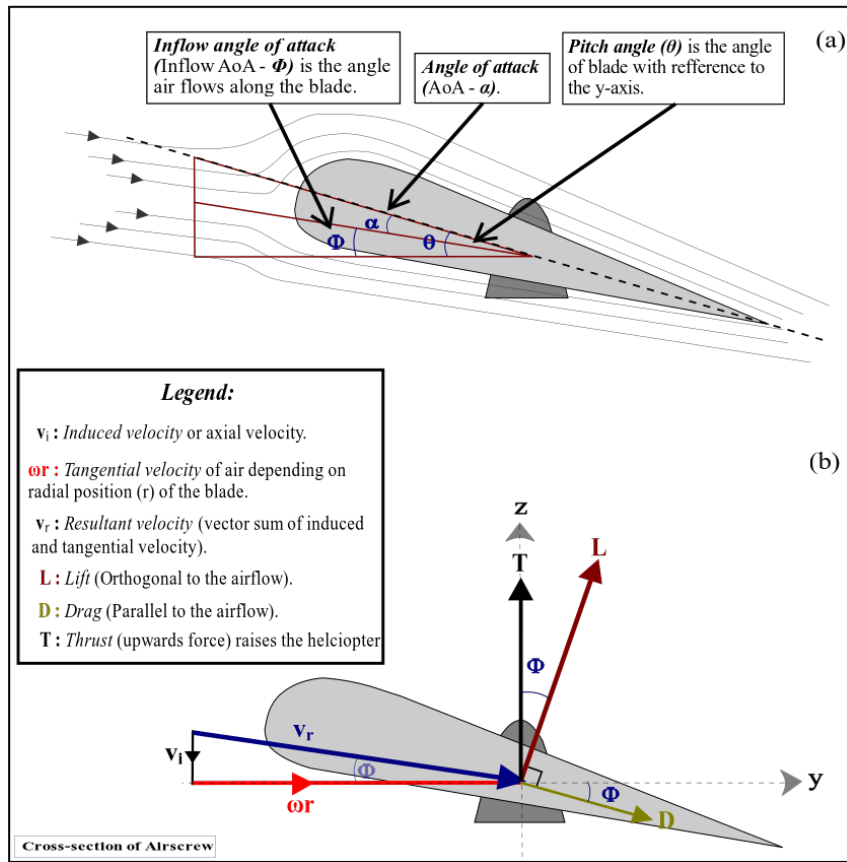


**Figure 4:** A diagram in which (a) deconstructs the angles in relation with the blades, (b) interprets the blades free body diagram.

The force perpendicular to airflow is lift ( $L$ ) and a new force parallel to airflow also exists, termed drag ( $D$ ), figure 4. The vertical component of lift and drag produces thrust. As the inflow AoA is insignificant ( $\phi \approx 0$ ), trigonometric ratios reduce to  $\cos \phi \rightarrow 1$  and  $\sin \phi \rightarrow 0$ . Hence, thrust approximately equals lift (16).

$$T = L \cos \phi + D \sin \phi$$

$$T \approx L \tag{16}$$

## 5 Determining Thrust Coefficient

Realise, the force orthogonal to airflow is lift, corresponding with Bernoulli's principle (2).

$$L = \frac{1}{2}A\rho\bar{v}^2$$

Substituting resultant velocity (15) in lift, we recognise as radial position ( $r$ ) increases from hub ( $r = 0$ ) to tip ( $r = R$ ), lift also increases with each blade element ( $dr$ ). This implies lift is non-uniformly produced along the blade. The blade element theory suggests, the cumulative sum of all blade elements is total lift and hence, we integrate (Gessow & Myers, 1985). Furthermore, the blade element area is rectangular and therefore product of infinitesimal length ( $dr$ ) and chord width ( $C$ ), figure 3.

$$L = \int_0^R \frac{1}{2}C\rho(\omega r)^2 dr$$

Incorporating an empirical factor known as lift coefficient ( $c_L$ ) allows accounting for NACA 0015 aerofoil geometry used in our experiment (see section 7). The lift coefficient is a first order function when mapped with AoA ( $\alpha$ ) and passes through origin ( $\alpha, c_L$ ) : (0,0) (Venkatesan, 2012). The function is  $y = mx \iff c_L = a\alpha$ , where 'a' is the lift-curve gradient. We make AoA subject of (13) and further substitute inflow AoA (14) for lift.

$$L = \int_0^R \frac{1}{2}C\rho(\omega r)^2 c_L dr = \int_0^R \frac{1}{2}C\rho(\omega r)^2 a\alpha dr$$

$$\alpha = \theta - \phi \implies \theta - \frac{v_i}{\omega r}$$

$$L = \int_0^R \frac{1}{2}C\rho(\omega r)^2 a\left(\theta - \frac{v_i}{\omega r}\right) dr$$

We simplify lift and remove constants outside the integral. Since, lift only considers force from one blade, multiplying by 2 yields total lift. As lift-thrust identity (15) holds true, total lift approximates thrust (17).

$$L = \frac{1}{2}C\rho a \int_0^R \theta(\omega r)^2 - v_i(\omega r) dr$$

$$T = C\rho a \int_0^R \theta(\omega r)^2 - v_i(\omega r) dr \quad (17)$$

Lastly, we can now determine the corrected thrust coefficient using (9), by substituting for corrected thrust (17). Realise by dividing the fraction, we obtain a new variable,  $\bar{r} = \frac{r}{R}$  (Venkatesan, 2012). Hence, boundary conditions change; lower limit  $\lim_{r \rightarrow 0} \bar{r} = 0$  and upper limit  $\lim_{r \rightarrow R} \bar{r} = 1$ .

$$c_T = \frac{T}{\rho\pi R^2(\omega R)^2} \implies \frac{C\rho a \int_0^R \theta(\omega r)^2 - v_i(\omega r) dr}{\rho\pi R^2(\omega R)^2}$$

$$c_T = \frac{Ca}{\pi R} \int_0^1 (\theta(\bar{r})^2 - \frac{v_i}{\omega R}(\bar{r})) d\bar{r}$$

To further simplify, we assume inflow AoA  $\phi = \frac{v_i}{\omega r} \approx \frac{v_i}{\omega R}$ . This assumption is valid as magnitude for tangential velocity along the blade ( $\omega r$ ) approximates to at the tip ( $\omega R$ ), since dynamic pressure is significantly larger at tip due to their proportionality. Substituting this approximation and solving the integral we obtain thrust coefficient (18).

$$c_T = \frac{Ca}{\pi R} \int_0^1 (\theta\bar{r}^2 - \phi\bar{r}) d\bar{r} = \frac{Ca}{\pi R} \left[ \frac{\theta\bar{r}^3}{3} - \frac{\phi\bar{r}^2}{2} \right]_0^1$$

$$c_T = \frac{Ca}{\pi R} \left( \frac{\theta}{3} - \frac{\phi}{2} \right) \quad (18)$$

Since, chord width ( $C = 0.0180 \pm 0.00500m$ ), radius of blade ( $R = 0.0900 \pm 0.00500m$ ) and pitch ( $\theta = 0.157 \pm 0.00900rad$ ) are measured variables in the experiment (see section 7), we require to know inflow angle of attack and lift-curve gradient to determine thrust coefficient.

## 5.1 Determining inflow angle of attack

We still assume  $\phi = \frac{v_i}{\omega r} \approx \frac{v_i}{\omega R}$  to keep inflow AoA constant with radial position, otherwise the investigation becomes convoluted. Notice, (10) from section 3 can be rearranged to the form  $\frac{v_i}{\omega R}$ , which by our assumption approximates inflow AoA.

$$v_i = \omega R \sqrt{\frac{c_T}{2}} \implies \phi \approx \frac{v_i}{\omega R} = \sqrt{\frac{c_T}{2}}$$

Substituting thrust coefficient (18) and lift-curve gradient,  $a = 2\pi$  (explained in section 5.2), we express inflow AoA as a quadratic.

$$\phi^2 = \frac{c_T}{2} = \frac{Ca}{2\pi R} \left( \frac{\theta}{3} - \frac{\phi}{2} \right)$$

$$\left( \frac{2\pi R}{Ca} \right) \phi^2 + \left( \frac{1}{2} \right) \phi - \frac{\theta}{3} = 0$$

$$\left( \frac{R}{C} \right) \phi^2 + \left( \frac{1}{2} \right) \phi - \frac{\theta}{3} = 0$$

Replacing values measured in experiment (see section 7) forms a quadratic (19).

$$5.00\phi^2 + 0.500\phi - 0.0520 = 0 \quad (19)$$

The steps for error propagation are demonstrated bellow.

Fractional uncertainty for numerator.	$\frac{\Delta R}{R} = \frac{0.00500}{0.0900} = 0.0560m$
Fractional uncertainty for denominator.	$\frac{\Delta C}{C} = \frac{0.00500}{0.0180} = 0.278m$
Sum of fractional uncertainties for numerator and denominator is that for coefficient of $\phi^2$ .	$\frac{\Delta R}{R} + \frac{\Delta C}{C} = 0.334$
Absolute uncertainty for coefficient, rounded to 3.sig.fig.	$\Delta \frac{R}{C} = 1.70m$
Fractional uncertainty for y-intercept equals fractional uncertainty for pitch.	$\frac{\Delta \theta}{\theta} = \frac{0.00900}{0.157} = 0.0573m$
Absolute uncertainty for y-intercept is rounded to 3.sig.fig similar to y-intercept.	$\Delta \frac{\theta}{3} = 0.00300m$

$$(5.00 \pm 0.170)\phi^2 + 0.500\phi - (0.0520 \pm 0.00300) = 0$$

We obtain an original, maximum, minimum value for inflow AoA after implementing the uncertainties and graphically solving them with domain  $(0, \infty)$ . The original quadratic (19) yields  $\phi = 0.0640rad$  (figure 5a).

$$5.00\phi^2 + 0.500\phi - 0.0520 = 0$$

The maximum quadratic yields  $\phi = 0.0740rad$  (figure 5b).

$$3.30\phi^2 + 0.500\phi - 0.0490 = 0$$

The minimum quadratic yields  $\phi = 0.0560rad$  (figure 5c).

$$6.70\phi^2 + 0.500\phi - 0.0550 = 0$$

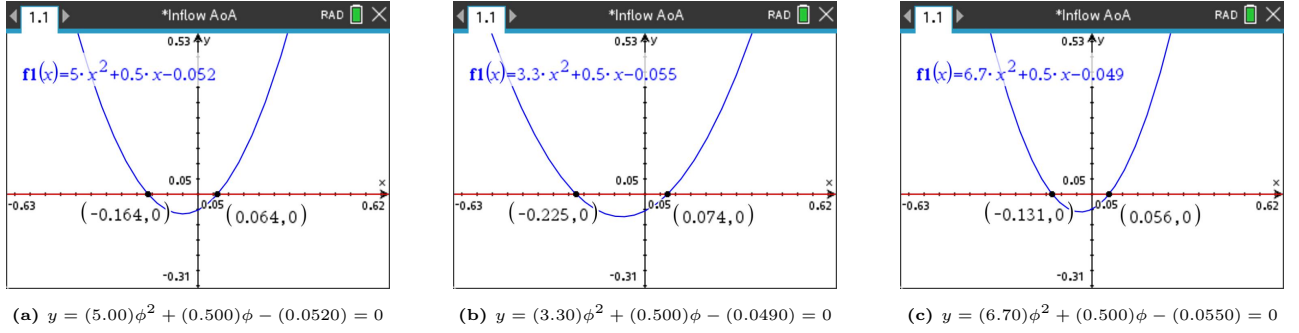


**Figure 5:** Graphs to determine inflow AoA ( $\phi$ ).

Hence, a good approximation for inflow AoA is the mean ( $\bar{\phi}$ ) of range and for uncertainty is unbiased standard deviation ( $\sigma_{\phi}$ ) demonstrated below.

$$\bar{\phi} = \frac{\phi_1 + \phi_2 + \phi_3}{3} = \frac{0.056 + 0.064 + 0.074}{3} = 0.0650$$

$$\sigma_{\phi} = \sqrt{\frac{(\phi_1 - \bar{\phi})^2 + (\phi_2 - \bar{\phi})^2 + (\phi_3 - \bar{\phi})^2}{N - 1}}$$

$$\sigma_{\phi} = \sqrt{\frac{(0.056 - 0.065)^2 + (0.064 - 0.065)^2 + (0.074 - 0.065)^2}{2}} = 0.00903$$

Therefore, inflow AoA,  $\phi = 0.0650 \pm 0.00903$  to 3.sig.fig.

## 5.2 Determining lift-curve gradient

The lift-curve gradient accounts for resistive forces caused by the blade's (aerofoil) geometry. Air resistance results from skin friction and form drag creating turbulence, figure 6. Turbulence decreases tangential velocity, proportionally decreasing dynamic pressure (Administration, 2020). By Froude's argument this decreases thrust.

The industrially averaged magnitude for lift-curve gradient is  $a = 2\pi$ , for all angular veloc-

ities and aerofoil (Scott, 2018). The lift-curve gradient of lift coefficient against AoA ( $c_L$  vs  $\alpha$ ) graph can be found using XFOIL; a fluid simulation programme. XFOIL develops unique environment for varying angular velocities of a rotor based on Reynolds number ( $Re$ ), which predicts airflow patterns (Halliday et al., 2014). After undergoing a mathematical process (see Appendix 1), Reynolds number is found using simplified form (20).

$$Re = 1266.98(\omega R) \tag{20}$$

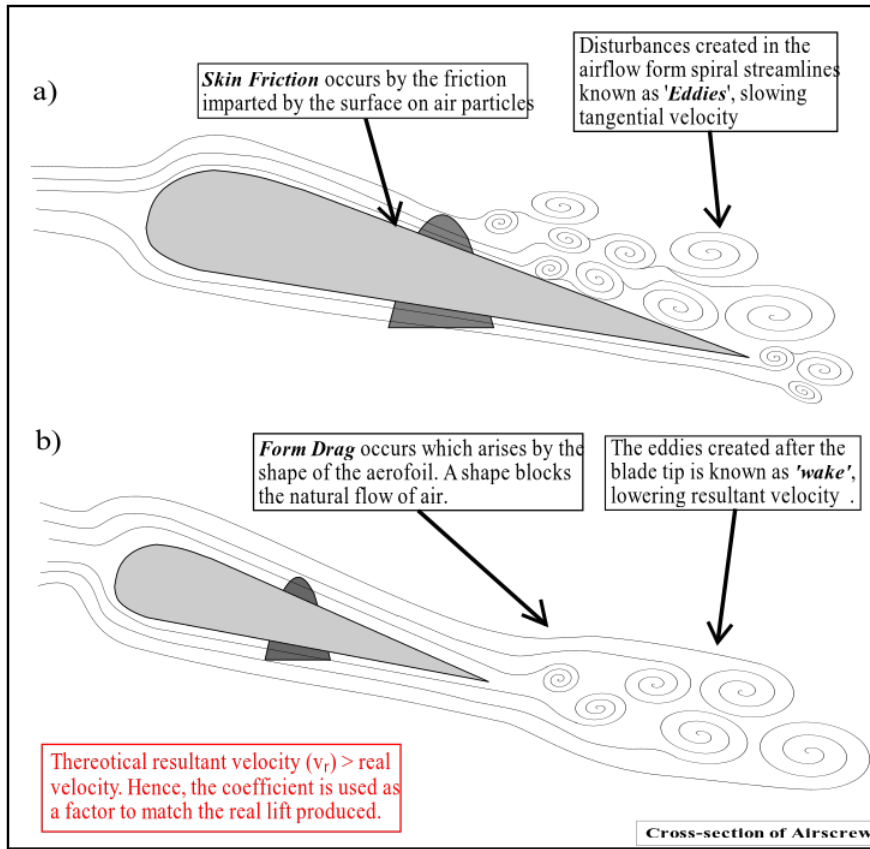


**Figure 6:** Air resistance forces which occur decreasing resultant velocity.

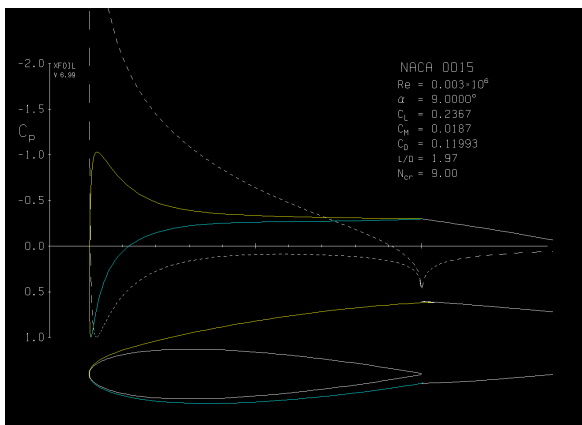
To determine Reynolds number, we require to define angular velocities to simulate in XFOIL. The experiment in section 7, uses revolutions per minute ( $RPM \text{ min}^{-1}$ ) as a relative measure for angular velocity. The experiment uses a motor with an operational range from 0 – 7000  $RPM$ , where tests are conducted in increments of 250  $RPM$ . We will therefore simulate within the operational range and the same increments.  $RPM$  determines frequency of revolution, hence conversion to angular velocity requires the factor  $\frac{2\pi}{60}$ . A sample set of conversions is shown in table 2, where values are rounded to  $RPM$  of lowest significant figure. Substituting angular velocities, we obtain Reynolds numbers displayed in sample table 2 (see

Appendix 2). Error propagation is unnecessary as XFOIL does not recognise error, decreasing confidence in lift-curve gradient.

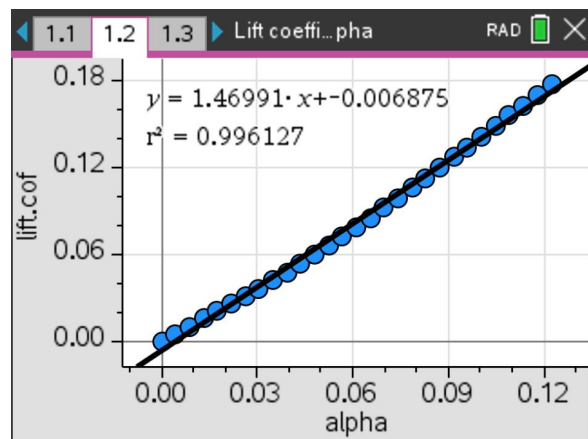
Revolutions per minute ( <i>RPM</i> )	Angular velocity ( $\omega$ )	Tangential velocity ( $\omega R$ )	Reynolds Number ( <i>Re</i> )
$/min^{-1}$	$/rad\ s^{-1}$	$/m\ s^{-1}$	-
0	0	0	0
250	26	2.4	3000
500	50	5	6000
750	79	7.1	9000
1000	100	10	10000
...	...	...	...

**Table 2:** A table determining Reynolds number

Reporting Reynolds number to XFOIL, a simulation is produced in one tab (see figure 7a) and a  $c_L$  vs  $\alpha$  table in the other. The table is then converted to a graph (see figure 7b), which uses  $26\ rad\ s^{-1}$  as an example. A linear regression line is graphed to verify linearity, which as indicated by Pearson correlation coefficient  $r = 0.998$  is very strong. However, a systematic error is observed as the regression line intersects y-axis at  $(\alpha, c_L) : (0, -0.007)$ , but not the origin. The difference between y-intercepts is negligible, hence the graph can be considered reliable. The lift-curve gradient for  $26\ rad\ s^{-1}$  is  $a = 1.47$  to 3.sig.fig. The remaining angular velocities are found with a similar process, shown in sample table 3 (see Appendix 3).



(a) An illustration of XFOIL simulation for  $26\ rad\ s^{-1}$ .



(b) A lift  $c_L$  vs  $\alpha^c$  graph.

**Figure 7:** Simulation and analysis of data from XFOIL.

Angular velocity ( $\omega$ )	Tangential velocity ( $\omega R$ )	Reynolds Number ( $Re$ )	Lift-curve gradient ( $a$ )
$/rad\ s^{-1}$	$/m\ s^{-1}$	-	-
0	0	0	0
26	2.4	3000	1.47
50	5	6000	1.28
79	7.1	9000	1.23
100	10	10000	1.22
...	...	...	...

**Table 3:** A table determining lift-curve gradient

Data from table 3 is quantitatively demonstrated as a graph in figure 8. The mean for all lift-curve gradient points is represented as a mean line ( $a_{theo} = 4.81$ ). An industrially agreed mean line is also illustrated ( $a_{emp} = 2\pi = 6.28$ ). The data points  $< a_{theo}$  ( $0 - 222\ rad\ s^{-1}$ ) shows a theoretically inefficient range, as a great proportion of work is lost to turbulence, which decreases dynamic pressure. Similarly, data points between  $a_{theo}$  and  $a_{emp}$  ( $222 - 240\ rad\ s^{-1}$  and  $431 - 733\ rad\ s^{-1}$ ) indicates an ideal range, as predominant amount of work is used to generate thrust. Lastly, data points  $> a_{emp}$  ( $240 - 431\ rad\ s^{-1}$ ) represents an efficient range, as resistive forces insignificantly impact dynamic pressure and therefore, most work generates thrust.

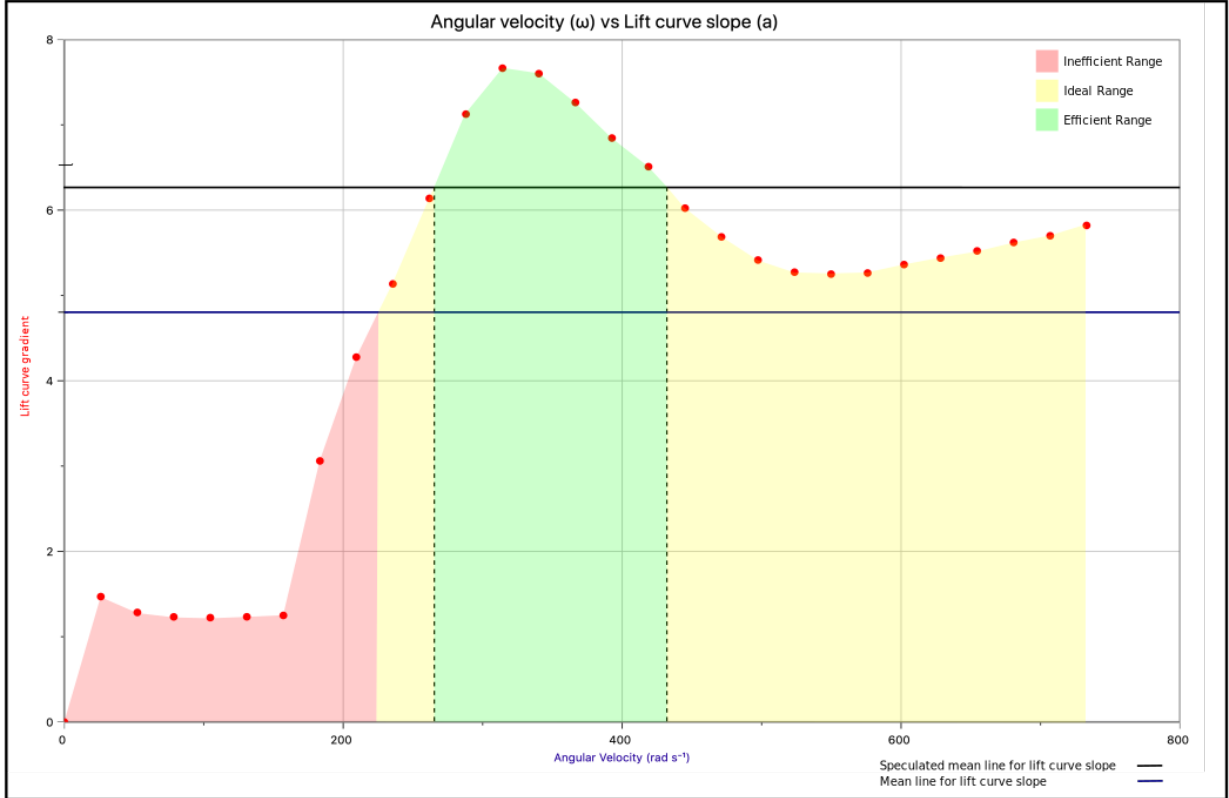


**Figure 8:** The relationship between angular velocity and lift-curve gradient.

### 5.3 Determining thrust coefficient

Recalling (18), we can now find the thrust coefficient with respect to angular velocity. However, the thrust coefficient is theoretically deduced and fails to recognise mechanical losses for e.g. bearing friction. This requires to implement a constant  $k = 1.75$  (Venkatesan, 2012).

$$c_T = k \frac{Ca}{\pi R} \left( \frac{\theta}{3} - \frac{\phi}{2} \right)$$

Substituting values for the variable's, we obtain thrust coefficient demonstrated in table 4 (see Appendix 4). The thrust coefficient is calculated to 3.sig.fig, as the variable with smallest significant figure. Uncertainty for the thrust coefficient are found with steps bellow.

<p>Fractional uncertainty for multiplicand (<math>\frac{Ca}{\pi R}</math>) is that for <math>\frac{C}{R}</math>, as other variables have zero uncertainty.</p> <p>Fractional uncertainty for <math>\frac{\theta}{3}</math> is that for pitch.</p> <p>Absolute uncertainty for <math>\frac{\theta}{3}</math>.</p> <p>Same steps for absolute uncertainty of <math>\frac{\phi}{2}</math>.</p> <p>Absolute uncertainty for <math>\frac{\theta}{3} - \frac{\phi}{2}</math>.</p> <p>Fractional uncertainty for multiplier.</p> <p>Fractional uncertainty for thrust coefficient is sum of the fractional uncertainty for multiplicand and multiplier.</p> <p>Percentage uncertainty for thrust coefficient</p>	<p><math>\frac{\Delta \frac{Ca}{\pi R}}{\frac{Ca}{\pi R}} = 0.334</math> derived from section 5.1.</p> <p><math>\frac{\Delta \theta}{\theta} = \frac{0.00900}{0.157} = 0.0573</math></p> <p><math>\Delta \frac{\theta}{3} = 0.00300</math></p> <p><math>\Delta \frac{\phi}{2} = 0.00400</math></p> <p><math>\Delta \frac{\theta}{3} - \frac{\phi}{2} = 0.00300 + 0.00400 = 0.00700</math></p> <p><math>\frac{\Delta \frac{\theta}{3} - \frac{\phi}{2}}{\frac{\theta}{3} - \frac{\phi}{2}} = \frac{0.00700}{0.0200} = 0.350</math></p> <p><math>\frac{\Delta c_T}{c_T} = 0.334 + 0.350 = 0.684</math></p> <p><math>\Delta c_T \% = 68.4\%</math></p>
--	---

Air screw geometry ( $R, C$ )	Air screw angles ( $\theta, \phi$ )	Angular velocity ( $\omega$ )	Lift-curve gradient ( $a$ )	Thrust coefficient ( $c_T$ )
/m	/rad	/rad s <sup>-1</sup>	-	-
$\pm 0.00500, \pm 0.00500$	$\pm 0.00900, \pm 0.00900$	-	-	68.4%
0.0900, 0.0180	0.157, 0.0650	0	0	0
		26	1.47	0.00359
		50	1.28	0.00313
		79	1.23	0.00301
		100	1.22	0.00299
		...	...	...

**Table 4:** A table demonstrating the thrust coefficient  $c_T$  based on it's constituent angular velocity ( $\omega$ ).

The data from table 4 is quantitatively represented as a graph in figure 9. The trend closely corresponds with lift-curve gradient against angular velocity graph in figure 8. The mean of all thrust coefficient data points is illustrated through a mean line. Although error bars are substantially large, the inefficient range is positioned below mean line and opposite is true for ideal and efficient ranges providing confidence with our speculations.

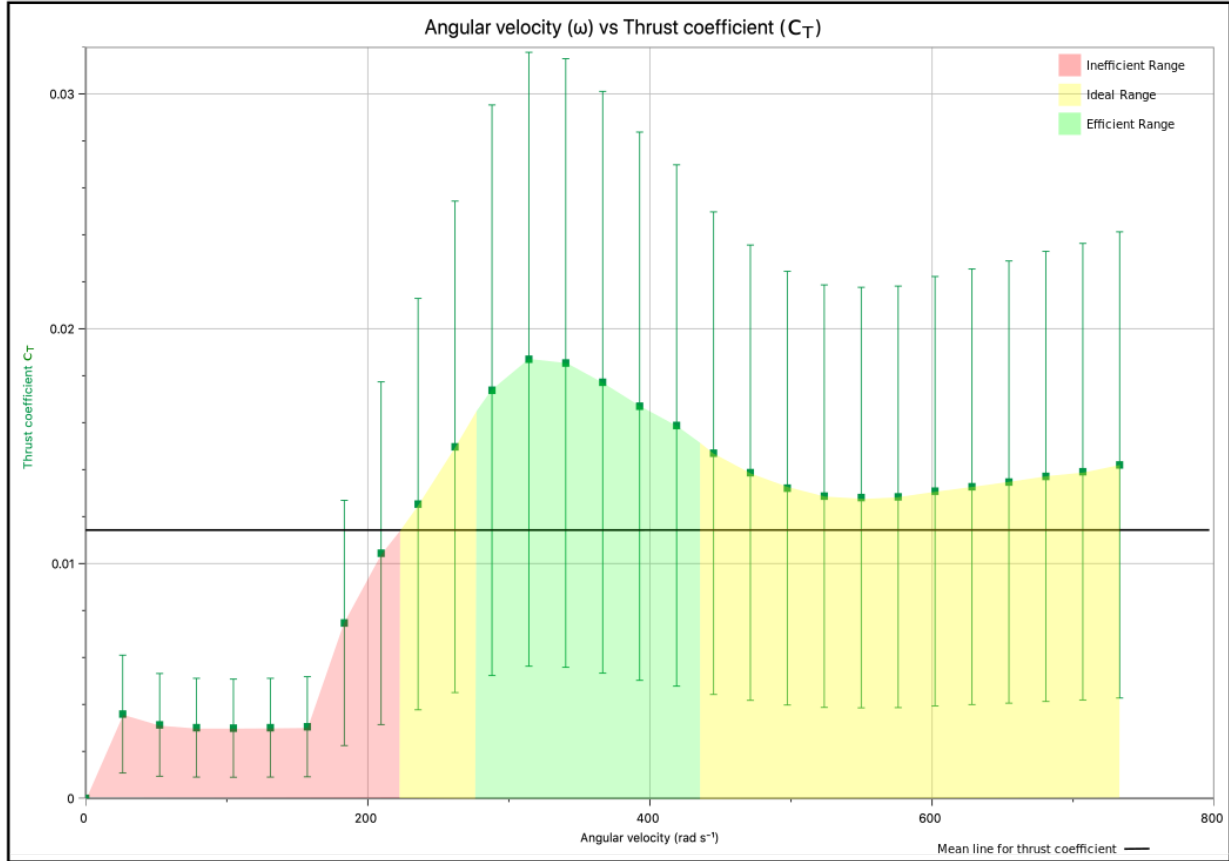


**Figure 9:** The relationship between angular velocity and thrust coefficient.

## 6 Determining Power Coefficient

The power determined in (7) is unsatisfactory, as it omits variables such as, resultant velocity and air resistance. Hence, we will consider a new approach, which focuses on the revolution of airscrew. Power is tangential force ( $F$ ) experienced by an aerofoil along a distance ( $s$ ) divided by time elapsed ( $\Delta t$ ) to travel the distance (see figure 10a).

$$\bar{P} = Fv = \frac{Fs}{\Delta t}$$

The magnitude of arc length travelled can be expressed as  $s = \beta R$ , where the aerofoil revolves an angle  $\beta$  in  $\Delta t$  time. Notice,  $\frac{\beta}{\Delta t}$  is definition of angular velocity. Power is therefore

product of tangential force and velocity.

$$\bar{P} = \frac{F\beta R}{\Delta t} = F(\omega R)$$

Additionally, considering air as frame of reference, tangential force is the horizontal component of lift and drag, figure 10b. The small angle approximation for inflow AoA simplifies  $\sin \phi \rightarrow \phi$  and  $\cos \phi \rightarrow 1$ . Lift and drag can be expanded using blade element theory, integrating along the blade's length. The expanded expression for drag is equivalent to lift, except for drag coefficient ( $c_D$ ) (Gessow & Myers, 1985).

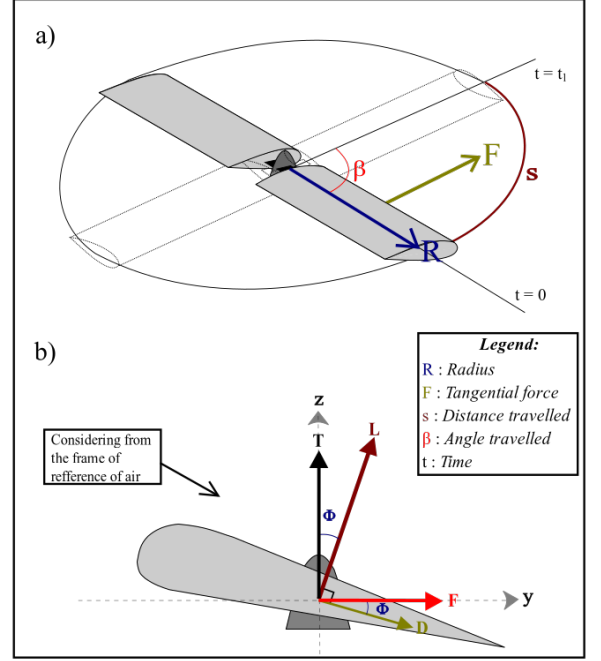


**Figure 10:** A modified approach for power coefficient.

$$\bar{P} = \omega R \left[ \int_0^R (L \sin \phi + D \cos \phi) dr \right] = \omega R \int_0^R (L \phi + D) dr$$

$$\bar{P} = \omega R \int_0^R \left( \frac{1}{2} C \rho (\omega r)^2 c_L \right) \phi dr + \int_0^R \frac{1}{2} C \rho (\omega r)^2 c_D dr$$

$$\bar{P} = \frac{1}{2} C \rho \omega R \left[ a \phi \int_0^R \theta(\omega r)^2 - v_i(\omega r) dr + \int_0^R (\omega r)^2 c_D dr \right]$$

We multiply power equation by two, in order to consider both blades (21). Substituting power within power coefficient from (9) and dividing by denominator, we observe the variable  $\bar{r} = \frac{r}{R}$ . The boundary conditions change (see Section 5).

$$\bar{P} = C \rho \omega R \left[ a \phi \int_0^R \theta(\omega r)^2 - v_i(\omega r) dr + \int_0^R (\omega r)^2 c_D dr \right] \quad (21)$$

$$c_P = \frac{\bar{P}}{\rho \pi R^2 (\omega R)^3} = \frac{C \rho \omega R \left[ a \phi \int_0^R \theta(\omega r)^2 - v_i(\omega r) dr + \int_0^R (\omega r)^2 c_D dr \right]}{\rho \pi R^2 (\omega R)^3}$$

$$c_P = \phi \int_0^1 \frac{C a}{\pi R} (\theta \bar{r}^2 - \phi \bar{r}) dr + \int_0^1 \frac{C}{\pi R} (\bar{r}^3 c_D) dr$$

Notice, the first integral simplifies to thrust coefficient (18). Solving the integral, we obtain power coefficient (22).

$$c_P = \phi c_T + \int_0^1 \frac{C}{\pi R} (\bar{r}^3 c_D) dr$$

$$c_P = \phi c_T + \frac{C}{4\pi R} c_D \quad (22)$$

The power coefficient can only be found, after determining drag coefficient.

## 6.1 Determining drag coefficient

The drag coefficient incorporates resistive forces acting on a NACA 0015 aerofoil. Similar to lift coefficient, drag coefficient is found using XFOIL. After inserting the calculated Reynolds numbers (table 3), a  $c_D$  vs  $\alpha$  table is generated. Since, AoA is  $\alpha = \theta - \phi = 0.157 - 0.0650 = 0.0920rad$ , we select drag coefficients at  $\alpha = 0.0920rad$  for all angular velocities displayed in sample table 5 to 3 sig.fig (see Appendix 5). Uncertainty is not calculated as XFOIL doesn't recognise error, decreasing confidence with drag coefficient.

Angular velocity ( $\omega$ )	Tangential velocity ( $\omega R$ )	Reynolds Number ( $Re$ )	Lift curve gradient ( $a$ )	Drag coefficient ( $c_D$ )
$/rad\ s^{-1}$	$/m\ s^{-1}$	-	-	-
0	0	0	0	0.0933
26	2.4	3000	1.47	0.0756
50	5	6000	1.28	0.0683
79	7.1	9000	1.23	0.0642
100	10	10000	1.22	0.0616
...	...	...	...	...

**Table 5:** A table demonstrating drag coefficient ( $c_D$ ) based on its constituent angular velocity ( $\omega$ ).

## 6.2 Determining power coefficient

We can now calculate power coefficient (22). Recall from section 5.3, in order to consider mechanical losses we incorporate constant  $k = 1.75$ .

$$c_P = k\left(\phi c_T + \frac{C}{4\pi R} c_D\right)$$

Substituting for the variables, we obtain power coefficient demonstrated in sample table 7 (see Appendix 6). Uncertainty calculations are displayed below to 3 sig.fig, similar to variable with lowest significant figure. However, we make an exception and increase significant figures of angular velocity to 3 sig.fig, for maximising accuracy and precision when analysing data.

<p>Fractional uncertainty for inflow AoA.</p> <p>Sum for the fractional uncertainties of <math>\phi</math> and <math>c_T</math> is that for <math>\phi c_T</math>.</p> <p>Absolute uncertainty for <math>\phi c_T</math> varies as <math>c_T</math> changes with angular velocity. Example for <math>\omega = 26.2</math> and rest shown in sample table 6.</p> <p>Fractional uncertainty for <math>\frac{C}{4\pi R}c_D</math> is equivalent to that for <math>\frac{C}{R}</math>.</p> <p>Absolute uncertainty for <math>\frac{C}{4\pi R}c_D</math> varies, as <math>c_D</math> changes with angular velocity. Example for <math>\omega = 26.2</math> and rest shown in sample table 6.</p> <p>Absolute uncertainty for <math>\phi c_T + \frac{C}{4\pi R}c_D</math> (22) is sum of the absolute uncertainties for <math>\phi c_T</math> and <math>\frac{C}{4\pi R}c_D</math>. Example for <math>\omega = 26.2</math> and rest shown in sample table 6.</p> <p>Fractional uncertainty for <math>\phi c_T + \frac{C}{4\pi R}c_D</math> is then allowed. Example for <math>\omega = 26.2</math> and rest shown in sample table 6.</p> <p>Fractional uncertainty for <math>\phi c_T + \frac{C}{4\pi R}c_D</math> is equivalent to that for <math>c_P</math>.</p> <p>Absolute uncertainty for <math>c_P</math> varies with <math>\omega</math>. Example for <math>\omega = 26.2</math> and rest shown in sample table 7.</p>	$\frac{\Delta\phi}{\phi} = \frac{0.00903}{0.0650} = 0.138rad$ $\frac{\Delta\phi c_T}{\phi c_T} = 0.138 + 0.684 = 0.822$ $\phi c_T = 0.000233 \quad \Delta\phi c_T = 0.000233(0.822) = 0.000195$ $\frac{\Delta\frac{C}{R}}{\frac{C}{R}} = 0.334 \text{ from section 5.1.}$ $\frac{C}{4\pi R}c_D = 0.00149 \quad \Delta\frac{C}{4\pi R}c_D = 0.00149(0.344) = 0.000496$ $\Delta\phi c_T + \frac{C}{4\pi R}c_D = 0.000195 + 0.000496 = 0.000691$ $\frac{\Delta\phi c_T + \frac{C}{4\pi R}c_D}{\phi c_T + \frac{C}{4\pi R}c_D} = \frac{0.000691}{0.00172} = 0.402$ $\frac{\Delta c_P}{c_P} = \frac{\Delta\phi c_T + \frac{C}{4\pi R}c_D}{\phi c_T + \frac{C}{4\pi R}c_D}$ $c_P = 0.00301 \quad \Delta c_P = 0.00301(0.402) = 0.00121$
---	---

$\omega$	$\phi c_T$	$\Delta\phi c_T$	$\frac{C}{4\pi R}c_D$	$\Delta\frac{C}{4\pi R}c_D$	$\phi c_T + \frac{C}{4\pi R}c_D$	$\Delta\phi c_T + \frac{C}{4\pi R}c_D$	$\frac{\Delta c_P}{c_P}$
26.2	0.000233	0.000195	0.00149	0.000496	0.00172	0.000691	0.402
52.4	0.000204	0.000170	0.00120	0.000402	0.00141	0.000572	0.407
78.5	0.000195	0.000164	0.00109	0.000363	0.00128	0.000526	0.411
104	0.000194	0.000162	0.00102	0.000341	0.00122	0.000504	0.414
...	...	...	...	...	...	...	...

**Table 6:** Determining the absolute uncertainties of variables

Angular velocity ( $\omega$ )	Power coefficient ( $C_P$ )	Absolute uncertainty $\Delta C_P$
$rads^{-1}$	-	-
0	0	0
26.2	0.00301	0.00121
52.4	0.00246	0.00100
78.5	0.00224	0.000921
104	0.00213	0.000881
...	...	...

**Table 7:** Determining the theoretical power coefficient and the coefficients absolute uncertainty

The data in table 7 is represented as a graph in figure 11. For a system to be power efficient, the thrust and power to area ratio must strictly maximise and minimise respectively. The mean of all power coefficient data points are represented as a mean line. The angular velocities between  $0 - 183rads^{-1}$  are power inefficient, as they demonstrate a low thrust (see figure 9), but a large power coefficient. This suggests most power is used to overcome resistive forces. Moreover, angular velocities between  $183 - 733rads^{-1}$  in retrospect are not power efficient, as

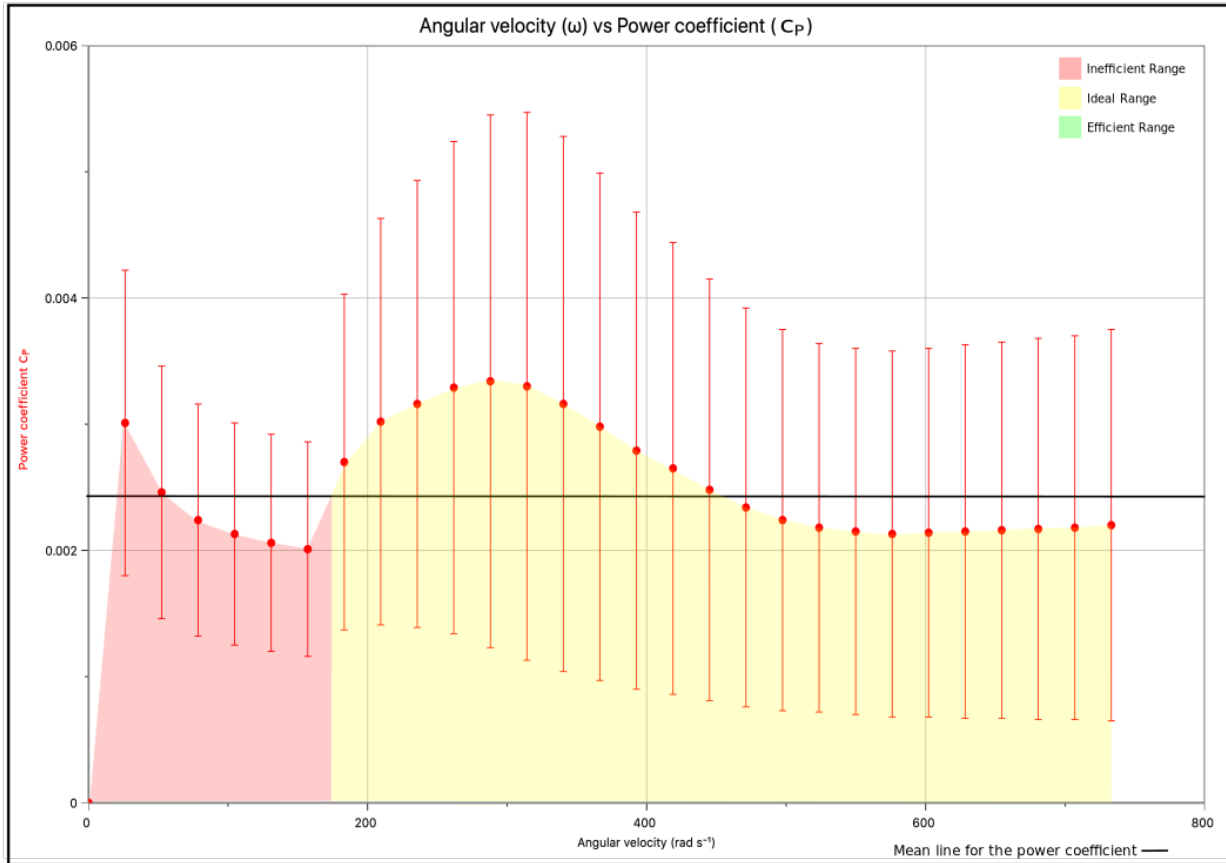


**Figure 11:** The relationship between angular velocity and power coefficient

they have a large thrust and power coefficient. Here, most power is used to generate thrust than lost to air resistance and therefore, has ideal efficiency contrary to speculations.

## 7 Determining Experimental Power Coefficient

I devised an experiment to observe power dissipated, later converted to power coefficient in revolving a twin bladed airscrew by a brushless DC motor (BLDC motor). Thrust measurements for determining thrust coefficient are not accounted, as the measuring scale provided misleading results (see figure 12). The experiment is necessary to validate whether theoretical data (see section 5.3 and 6.2) corresponds with experimental data. This is important, to find a reason for large error bars seen with the coefficients, sources of error or confounding variables.

### 7.1 Experimental Setup

In 1920-33, the National Advisory Committee for Aeronautics (NACA) designed and tested various standardised aerofoils (Allen, 2017). I selected their NACA 0015 aerofoil, for its symmetric geometry and ease to 3D print. The aerofoil was printed with dimensions stated in table 8 and went on top of BLDC motor.

Aerofoil Geometry	Properties
NACA 0015	Blade length: Radius $R = 0.0900 \pm 0.00500m$ Blade length: Chord width $C = 0.0180 \pm 0.00500m$ Total angle: Pitch angle $\theta = 0.157 \pm 0.00900rad$

**Table 8:** A description for the properties of NACA 0015 aerofoil

The experiment setup is represented in figure 12. An Arduino Mega 2560 microcontroller used a preloaded code (see Appendix 9) to change RPM of motor (Nedelkovski, 2019). A tachometer measures the frequency of reflections from a reflective adhesive on the motor, to determine the motors RPM. A power analyser measured the total power used by load. A camera positioned above the setup, recorded the displayed readings.

### 7.2 Experiment procedure

- **Independent variable:** Angular velocity measured in RPM.
- **Dependent variable:** Power dissipated in the system.

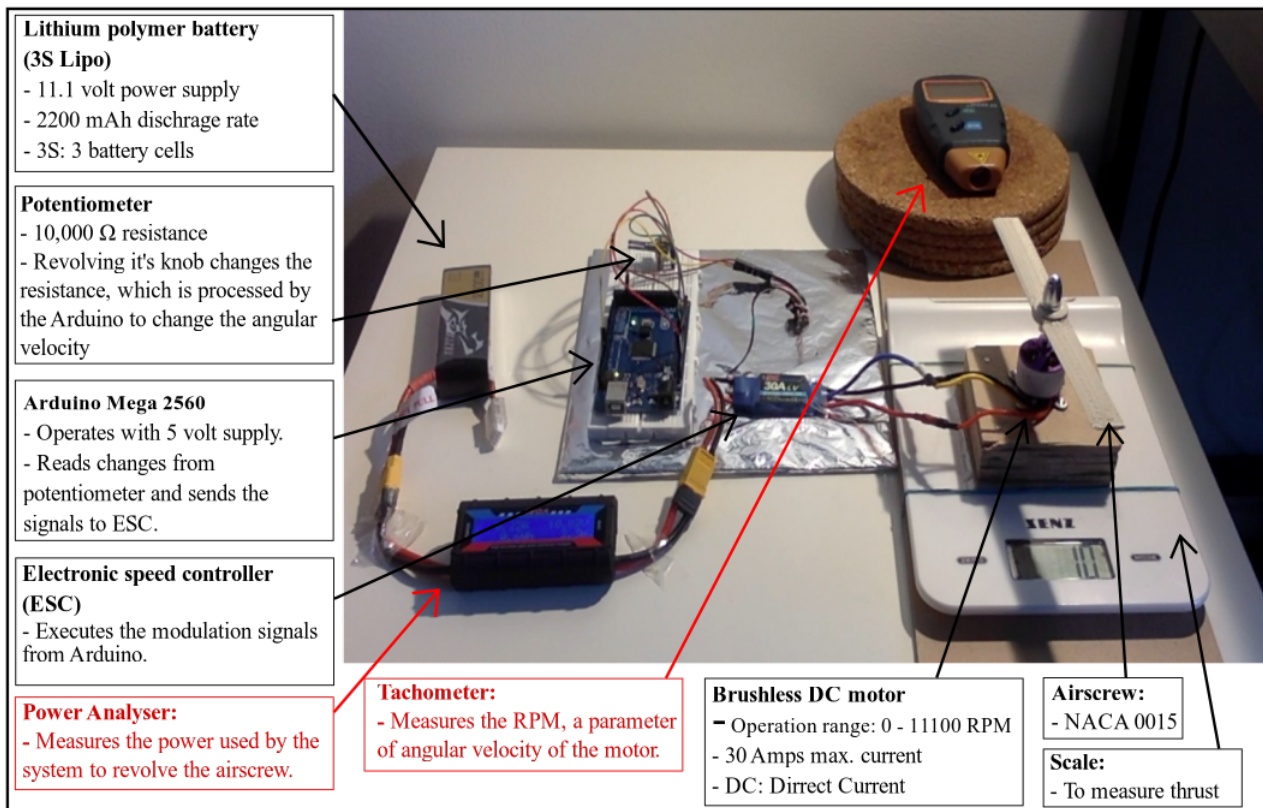


**Figure 12:** The experimental setup for determining the power coefficient.

A physical limitation of the motor is, it harshly vibrated between  $0 < \omega \leq 314 \text{rads}^{-1}$  and  $681 \leq \omega < 733 \text{rads}^{-1}$  deviating the photo tachometer readings. I realised to minimise systematic error, the testing range should be between  $314 \leq \omega \leq 681 \text{rads}^{-1}$ . Additionally, the angular velocity readings never remained constant while performing preliminary tests. Hence, I decided the experiment would be conducted in intervals of 250RPM ( $26.2 \text{rads}^{-1}$ ) beginning from  $301 < \omega \leq 327 \text{rads}^{-1}$  and ending with  $668 < \omega \leq 694 \text{rads}^{-1}$ . Each interval would be tested 5 times, for 15 seconds with a stopwatch. The data was collected from video recordings and is displayed in Appendix 7.

### 7.3 Theoretical vs experimental power coefficient

The RPM were converted to angular velocity using the factor  $\frac{2\pi}{60}$  (see Section 5.2). The angular velocities of an interval is best demonstrated by the mean. The mean for power measured within the interval, is suitable for the same reasoning. Such means are demonstrated in sample table 9 for first 5 intervals. Recall, the power coefficient (9). Substituting the values from table 9 yields the experimental power coefficient, also shown in sample table 9.

$$c_P = \frac{\bar{P}}{\rho\pi R^2(\bar{\omega}R)^3}$$

Angular velocity	Mean angular velocity ( $\bar{\omega}$ )	Mean power ( $\bar{P}_{avg}$ )	Experimental power coefficient ( $c_P$ )
$rads^{-1}$	$rads^{-1}$	$kgm^2s^{-3}$	-
$301 < \omega \leq 327$	318	2.8	0.00389
$327 < \omega \leq 353$	343	3.4	0.00363
$353 < \omega \leq 380$	367	3.7	0.00326
$380 < \omega \leq 406$	397	4.3	0.00302
$406 < \omega \leq 432$	420	4.9	0.00290
...	...	...	...

**Table 9:** Determining the experimental power coefficient.

The experimental and theoretical data points from table 7 and 9 are illustrated as a graph in figure 13, with ordinates drawn to indicate the experimented range. Both curves are close to perfect fit, as the experimental outcomes are more exaggerated deviating around 314 and  $680rads^{-1}$ . Nevertheless, both power coefficients have similar properties such as, a curve fit

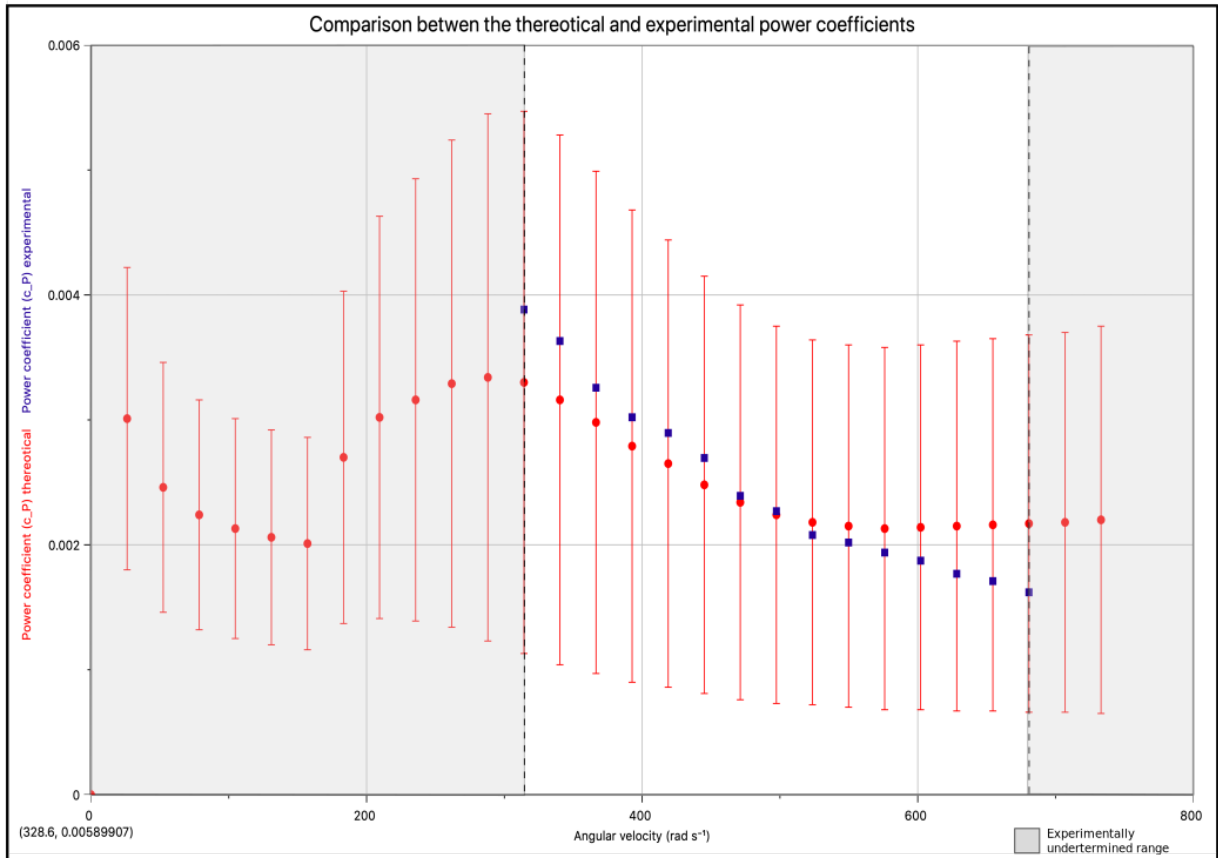


**Figure 13:** An analysis between angular velocity and power coefficient

which monotonically decreases with angular velocity. Their gradient ( $\frac{dc_P}{d\omega}$ ) converges to 0 from 550 to 600  $rad\,s^{-1}$  as both curves either seem to or form a plateau. Error bars are also useful, as experimental data follows the trend well within the error bars of theoretical data. Hence, the theoretical model closely resembles outcomes from experiment.

## 8 Determining Power Efficiency

Realise, we can finally determine power efficiency (11). Substituting the trust and power coefficient, yields power efficiency displayed in sample table 10 (see Appendix 8).

$$\eta = 70.7 \times \frac{c_T^{\frac{3}{2}}}{c_P}$$

Uncertainty for power efficiency is propagated with steps displayed below.

<p>Fractional uncertainty for numerator <math>c_T^{\frac{3}{2}}</math>.</p> <p>Fractional uncertainty for denominator <math>c_P</math> is demonstrated in table 6</p> <p>Fractional uncertainty for power efficiency (<math>\eta</math>) is sum of the fractional uncertainties for numerator <math>c_T^{\frac{3}{2}}</math> and denominator <math>c_P</math>. An example is <math>\omega = 26.2\,rad\,s^{-1}</math> and rest are shown in table 10.</p> <p>The absolute uncertainty for power efficiency can then be found. An example is <math>\omega = 26.2\,rad\,s^{-1}</math> and rest are shown in table 10.</p>	$\frac{\Delta c_T^{\frac{3}{2}}}{c_T^{\frac{3}{2}}} = \frac{3}{2} \left( \frac{\Delta c_T}{c_T} \right) = 1.50(0.684) = 1.09$  $\frac{\Delta \eta}{\eta} = \frac{\Delta c_T^{\frac{3}{2}}}{c_T^{\frac{3}{2}}} + \frac{\Delta c_P}{c_P} = 1.09 + 0.00301 = 1.49$  $\eta = 5.05 \quad \Delta \eta = 5.05(1.49) = 7.54$
--	--

Angular velocity ( $\omega$ )	Power efficiency ( $\eta$ )	Fractional uncertainty ( $\frac{\Delta \eta}{\eta}$ )	Absolute uncertainty ( $\Delta \eta$ )
$rad\,s^{-1}$	$kg\,m^2\,s^{-3}$	-	$kg\,m^2\,s^{-3}$
26.2	5.05	1.49	7.54
52.4	5.04	1.50	7.54
78.5	5.20	1.50	7.80
105	5.42	1.50	8.15
...	...	...	...

**Table 10:** Calculations for determining the power efficiency of our twin bladed single rotor helicopter system.

Table 10 is then converted to a power efficiency against angular velocity graph in figure 14. The general trend line increases and plateaus in a regular succession. Power efficiency at

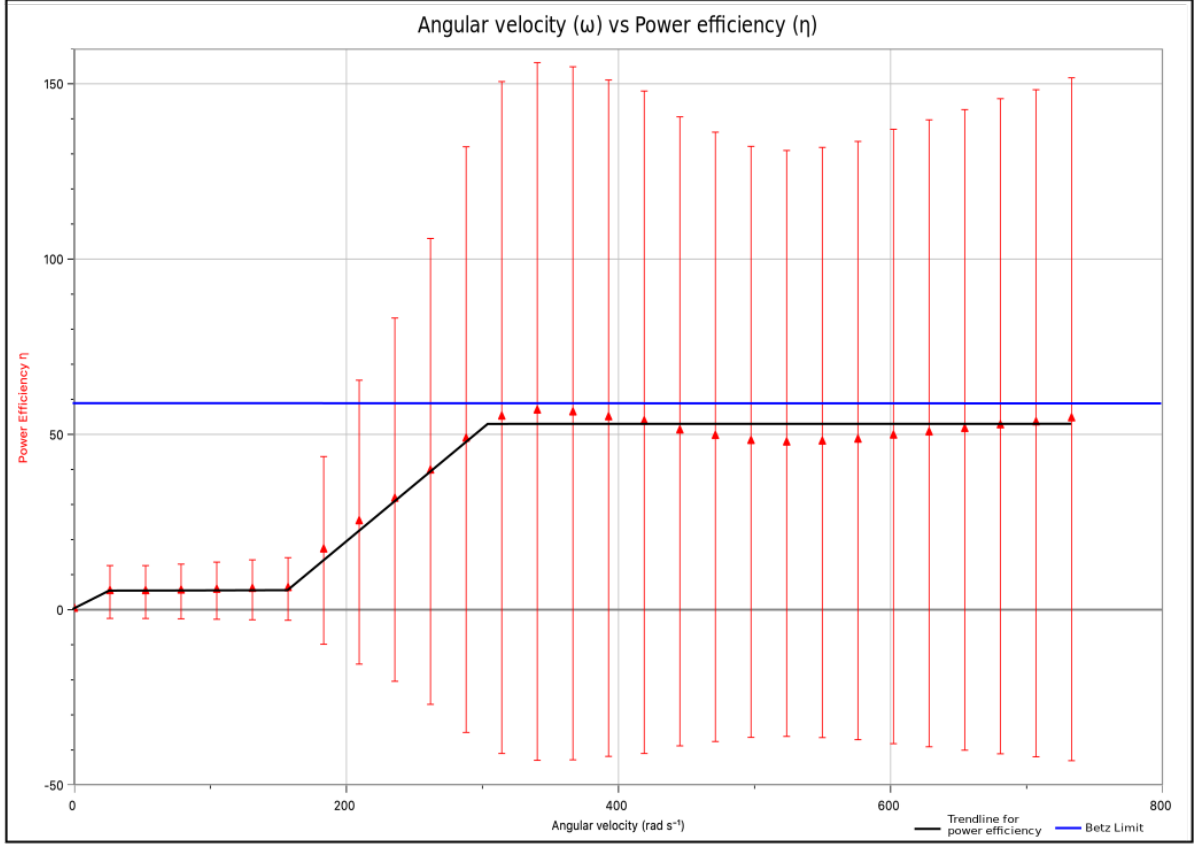


**Figure 14:** The relationship between power efficiency and angular velocity.

smaller angular velocities ( $0-157\text{rad s}^{-1}$ ) are an order of magnitude inefficient than at larger ones ( $314-733\text{rad s}^{-1}$ ) confirming the inefficient and ideal ranges, respectively. The maximum efficiency peaks at 54.6%, just under the maximum possible efficiency by Betz limit at 59.3% (Burton, 2009). Negative uncertainties cannot exist. As aforementioned, large uncertainties are caused by exhaustively using multiple equations to reach this relationship. Hence, the data quality is not compromised.

## 9 Evaluation and Conclusion

In investigating the research question, we decided to determine power efficiency with the thrust and power coefficient, resulting in many interesting observations.

Firstly, we found a limitation with Froude’s model, in that it assumed a zero pitch system, omitting internal forces and velocities. Hence, modifications such as blade element theory were made to implement pitch, enhancing the correlation between empirical and theoretical data.

In determining the thrust coefficient, XFOIL allowed to find lift-curve gradient and an analysis with industrial specification. This categorised angular velocity into an inefficient, ideal and efficient range, where smaller angular velocities in comparison to larger angular velocities required a substantial amount of power to overcome resistive forces. The power coefficient showed similar efficiencies, except for the efficient range. The experiment validated the theoretical ranges and also realised the large uncertainties were of a purely mathematical consequence. Hence, the inefficient and ideal ranges were confirmed as maximum power efficiency peaked only at 54.6%. However, a limitation with experiment was the small experimented range, not allowing a full comparison with theoretical model.

In conclusion a clear proportionality is visible between angular velocity and power efficiency for a twin bladed single rotor helicopter in hover. As we increase angular velocity, power efficiency increases then plateaus and repeats the same trend once again.

This investigation is not completely accurate, due to uncertainties and limitations. A part of these uncertainties arise from assumptions made with the theoretical model. For instance, assuming thrust linearly increases along the blade. Empirically, the tip produces negligible thrust, as the substantial dynamic pressure differential occurs from 20 to 80% of the blade (Administration, 2020). Secondly, a vortex known as induced drag is formed at the blade's tip, which moderately increases air resistance. This was not implemented in XFOIL adding unaccounted systematic error (Administration, 2020). Thirdly, the motor harshly vibrated at the first ( $301 < \omega \leq 327 \text{rads}^{-1}$ ) and last interval ( $668 < \omega \leq 694 \text{rads}^{-1}$ ), influencing the tachometer and power analyser, causing random error in data. This may explain deviations at start and end of the experimental power coefficient. However, I realised, seeking for a perfect match with experimental data is ambitious, as the investigation then becomes an extraneous mathematical process, reducing its ability to explain physics.

This investigation raises many questions, including one which initially inspired me: what angular velocity against power efficiency relationship can geometrically varied aerial vehicles such as, bi-copter and tri-copter demonstrate? Irregularly positioning rotor systems, makes the slipstream geometry unique and transcends the scope of this investigation. Many interesting problems arise, as the rotors must produce variable thrust to balance while hovering. Such an investigation would be incredibly interesting.

## 10 Works Cited

- Administration, F. (2020). *Rotorcraft Flying Handbook* (pp. 2-28). BN Publishing.
- Allen, B. (2017). *NACA Airfoils*. National Aeronautics and Space Administration. Retrieved 24 December 2020, from <https://www.nasa.gov/image-feature/langley/100/naca-airfoils>.
- Burton, T. (2009). *Wind energy* (1st ed., p. 6). Wiley.
- Gessow, A., & Myers, G. (1985). *Aerodynamics of the helicopter* (8th ed., pp. 46-65). Ungar.
- Halliday, D., Resnick, R., Walker, J., & Halliday, D. (2014). *Fundamentals of physics* (11th ed., pp. 386-412). Wiley.
- Helicopter Career Info*. Heliventures.co. (2017). Retrieved 4 September 2020, from <https://www.heliventures.co/new-helicopter-pilot-resources/helicopter-career-info/>.
- Lombardi, F. (2017). *Understanding Helicopter Power Requirements: The Power Struggle - Rotor & Wing International*. Rotor & Wing International. Retrieved 25 December 2020, from <https://www.rotorandwing.com/2017/10/10/understanding-helicopter-power-requirements-power-struggle/>.
- Nedelkovski, D. (2019). *Arduino Brushless Motor Control Tutorial*. HowToMechatronics. Retrieved 26 June 2020, from <https://howtomechatronics.com/tutorials/arduino/arduino-brushless-motor-control-tutorial-esc-bldc/>.
- Scott, J. (2018). *Lift Coefficient & Thin Airfoil Theory*. Aerospaceweb. Retrieved 28 November 2020, from [http://www.aerospaceweb.org/question/aerodynamics/q0136.shtml#:~:text=According%20to%20the%20ideal%20aerodynamics,%CE%B1\)%20is%20equal%20to%202%CF%80.&text=According%20to%20Thin%20Airfoil%20Theory,\(CL\)%20goes%20up](http://www.aerospaceweb.org/question/aerodynamics/q0136.shtml#:~:text=According%20to%20the%20ideal%20aerodynamics,%CE%B1)%20is%20equal%20to%202%CF%80.&text=According%20to%20Thin%20Airfoil%20Theory,(CL)%20goes%20up).
- Venkatesan. (2012). *Hovering Theory: Blade Element Theory*. Lecture, Indian Institute of Technology Kanpur.
- Zhao, D., Han, N., Goh, E., Cater, J., & Reinecke, A. (2019). *Wind turbines and aerodynamics energy harvesters* (pp. 1-5). Elsevier.

# 11 Appendix

## 11.1 Appendix 1: Simplifying Reynolds Number

Reynolds number measures airflow patterns, based on the properties of air. In fluid mechanics one form Reynolds number can take is displayed below. Here,  $\nu$  is kinematic viscosity,  $v_R$  is resultant velocity of airfoil and  $C$  is chord length. Kinematic viscosity of air at sea level and normal room temperature is:  $\nu = 1.42 \times 10^{-5}$ .

$$Re = \frac{Cv}{\nu}$$

We substitute the value for variables from section 7 and use resultant velocity (15).

However, realise  $v_R = \omega r \approx \omega R$ , as dynamic pressure is substantially large at the tip and approximately equal to that across the blade. Hence, by venturi effect tangential velocity at tip is also approximately equal to that across the blade.

$$Re = \frac{(0.0180)\omega r}{0.0000142}$$

$$Re = \frac{(0.0180)\omega R}{0.0000142} = 1266.98\omega R$$

## 11.2 Appendix 2: Conversion between Angular Velocity and Reynolds Number

<b>Revolution per minute (RPM)</b>	<b>Angular velocity (<math>\omega</math>)</b>	<b>Tangential velocity (<math>\omega R</math>)</b>	<b>Reynolds Number (Re)</b>
<i>/min<sup>-1</sup></i>	<i>/rads<sup>-1</sup></i>	<i>/ms<sup>-1</sup></i>	-
0	0	0.0	0
250	26	2.4	2991
500	52	4.7	5982
750	79	7.1	8972
1000	105	9.4	11963
1250	131	11.8	14954
1500	157	14.1	17945
1750	183	16.5	20935
2000	209	18.8	23926
2250	236	21.2	26917
2500	262	23.6	29908
2750	288	25.9	32899
3000	314	28.3	35889
3250	340	30.6	38880
3500	367	33.0	41871
3750	393	35.3	44862
4000	419	37.7	47853
4250	445	40.1	50843
4500	471	42.4	53834
4750	497	44.8	56825
5000	524	47.1	59816
5250	550	49.5	62806
5500	576	51.8	65797
5750	602	54.2	68788
6000	628	56.5	71779
6250	654	58.9	74770
6500	681	61.3	77760
6750	707	63.6	80751
7000	733	66.0	83742

### 11.3 Appendix 3: Determination of Lift-curve Gradient

<b>Angular velocity (<math>\omega</math>)</b>	<b>Tangential velocity (<math>\omega R</math>)</b>	<b>Reynolds Number (Re)</b>	<b>Lift-curve gradient (a)</b>
<i>/rads<sup>-1</sup></i>	<i>/ms<sup>-1</sup></i>	-	-
0	0.0	0	0.00
26	2.4	2991	1.47
52	4.7	5982	1.28
79	7.1	8972	1.23
105	9.4	11963	1.22
131	11.8	14954	1.23
157	14.1	17945	1.25
183	16.5	20935	3.06
209	18.8	23926	4.28
236	21.2	26917	5.14
262	23.6	29908	6.14
288	25.9	32899	7.13
314	28.3	35889	7.66
340	30.6	38880	7.60
367	33.0	41871	7.26
393	35.3	44862	6.84
419	37.7	47853	6.51
445	40.1	50843	6.02
471	42.4	53834	5.69
497	44.8	56825	5.42
524	47.1	59816	5.27
550	49.5	62806	5.25
576	51.8	65797	5.26
602	54.2	68788	5.36
628	56.5	71779	5.44
654	58.9	74770	5.52
681	61.3	77760	5.62
707	63.6	80751	5.70

#### 11.4 Appendix 4: Determination of Thrust Coefficient

Air screw geometry ( $R, C$ )	Aircrew Angles ( $\theta, \phi$ )	Angular velocity ( $\omega$ )	Gradient of lift-curve ( $a$ )	Thrust Coefficient ( $c_T$ )
$/m$	$/rad$	$/rads^{-1}$	-	-
$\pm 0.00500, \pm 0.00500$	$\pm 0.00900, \pm 0.00900$	-	-	<b>68.40%</b>
0.0900, 0.0180	0.157, 0.0650	0	0.00	0.00000
		26	1.47	0.00359
		52	1.28	0.00313
		79	1.23	0.00301
		105	1.22	0.00299
		131	1.23	0.00301
		157	1.25	0.00305
		183	3.06	0.00747
		209	4.28	0.01044
		236	5.14	0.01253
		262	6.14	0.01497
		288	7.13	0.01738
		314	7.66	0.01870
		340	7.60	0.01854
		367	7.26	0.01772
		393	6.84	0.01670
		419	6.51	0.01588
		445	6.02	0.01470
		471	5.69	0.01387
		497	5.42	0.01321
		524	5.27	0.01287
		550	5.25	0.01281
		576	5.26	0.01284
602	5.36	0.01308		
628	5.44	0.01327		
654	5.52	0.01347		
681	5.62	0.01371		
707	5.70	0.01391		
733	5.82	0.01420		

## 11.5 Appendix 5: Determination of Drag Coefficient

Angular velocity ( $\omega$ )	Tangential velocity ( $\omega R$ )	Reynolds Number (Re)	Lift-curve gradient (a)	Drag coefficient ( $c_D$ )
$/rads^{-1}$	$/ms^{-1}$	-	-	-
0	0.0	0	0.00	0.0000
26	2.4	2991	1.47	0.0933
52	4.7	5982	1.28	0.0756
79	7.1	8972	1.23	0.0683
105	9.4	11963	1.22	0.0642
131	11.8	14954	1.23	0.0616
157	14.1	17945	1.25	0.0598
183	16.5	20935	3.06	0.0664
209	18.8	23926	4.28	0.0658
236	21.2	26917	5.14	0.0623
262	23.6	29908	6.14	0.0568
288	25.9	32899	7.13	0.0490
314	28.3	35889	7.66	0.0421
340	30.6	38880	7.60	0.0376
367	33.0	41871	7.26	0.0345
393	35.3	44862	6.84	0.0321
419	37.7	47853	6.51	0.0302
445	40.1	50843	6.02	0.0289
471	42.4	53834	5.69	0.0275
497	44.8	56825	5.42	0.0266
524	47.1	59816	5.27	0.0256
550	49.5	62806	5.25	0.0249
576	51.8	65797	5.26	0.0241
602	54.2	68788	5.36	0.0235
628	56.5	71779	5.44	0.0229
654	58.9	74770	5.52	0.0224
681	61.3	77760	5.62	0.0219
707	63.6	80751	5.70	0.0215

## 11.6 Appendix 6: Determination of Power Coefficient

<b>Angular velocity (<math>\omega</math>)</b>	<b>Power coefficient (<math>c_p</math>)</b>	<b>Absolute uncertainty <math>\Delta c_p</math></b>
<i>/rads<sup>-1</sup></i>	-	-
0	0	0
26	0.00172	0.001209
52	0.00141	0.001001
79	0.00128	0.000921
105	0.00122	0.000881
131	0.00118	0.000860
157	0.00115	0.000847
183	0.00154	0.001328
209	0.00173	0.001605
236	0.00181	0.001772
262	0.00188	0.001954
288	0.00191	0.002111
314	0.00188	0.002172
340	0.00180	0.002116
367	0.00170	0.002008
393	0.00160	0.001889
419	0.00151	0.001793
445	0.00142	0.001668
471	0.00134	0.001576
497	0.00128	0.001505
524	0.00124	0.001463
550	0.00123	0.001451
576	0.00122	0.001447
602	0.00122	0.001464
628	0.00123	0.001476
654	0.00123	0.001491
681	0.00124	0.001510
707	0.00125	0.001524

## 11.7 Appendix 7: Raw Experimental Data

#	2875 < rpm ≤ 3125	Power	3125 < rpm ≤ 3375	Power	3375 < rpm ≤ 3625	Power	3625 < rpm ≤ 3875	Power
1	3017	2.9	3267	3.2	3417	3.3	3736	4.2
2	3017	3.1	3269	3.3	3434	3.5	3737	4.3
3	3018	3.0	3269	3.3	3436	3.1	3738	4.4
4	3019	3.3	3270	3.3	3445	3.5	3739	4.2
5	3020	3.1	3271	3.4	3447	3.8	3740	4.3
6	3022	2.7	3271	3.3	3450	3.8	3740	4.3
7	3022	2.8	3272	3.4	3453	3.5	3742	4.4
8	3023	2.9	3272	3.4	3453	3.7	3742	4.3
9	3029	2.8	3272	3.3	3459	3.7	3743	4.3
10	3030	2.8	3273	3.1	3460	3.7	3753	4.2
11	3039	3.2	3275	3.4	3461	3.6	3758	4.3
12	3040	3.2	3276	3.4	3462	3.8	3759	4.1
13	3042	2.4	3277	3.4	3464	3.6	3760	4.3
14	3042	3.0	3278	3.3	3472	3.3	3761	4.2
15	3043	2.7	3282	3.3	3474	3.8	3761	4.2
16	3043	2.7	3292	3.6	3478	4.0	3761	4.2
17	3044	2.4	3296	3.4	3496	3.8	3762	4.2
18	3044	2.8	3298	3.3	3500	3.3	3764	4.4
19	3044	2.6	3298	3.6	3516	3.7	3765	4.2
20	3045	2.4	3299	3.4	3517	3.4	3765	4.2
21	3045	2.8	3300	3.4	3518	3.8	3766	4.3
22	-		-	-	3536	3.6	3767	4.2
23	-	-	-	-	3538	3.6	3768	4.3
24	-	-	-	-	3540	3.8	3773	4.4
25	-	-	-	-	3541	3.8	3851	4.5
26	-	-	-	-	3546	3.8	3854	4.3
27	-	-	-	-	3547	3.7	3855	4.3
28	-	-	-	-	3548	3.7	3855	4.4
29	-	-	-	-	3548	3.7	3856	4.4
30	-	-	-	-	3548	3.8	3857	4.4
31	-	-	-	-	3549	3.8	3863	4.4
32	-	-	-	-	3549	3.9	3864	4.4
33	-	-	-	-	3550	3.8	3866	4.4
34	-	-	-	-	3552	3.8	3867	4.4
35	-	-	-	-	3553	3.6	3867	4.4
36	-	-	-	-	3556	3.8	3875	4.4
37	-	-	-	-	3559	3.8	-	-
38	-	-	-	-	3567	3.8	-	-
39	-	-	-	-	3575	3.9	-	-

#	3875 < rpm ≤ 4125	Power	4125 < rpm ≤ 4375	Power	4375 < rpm ≤ 4625	Power	4625 < rpm ≤ 4875	Power
1	3964	4.9	4141	5.5	4478	5.6	4699	6.4
2	3965	4.9	4157	5.2	4479	5.7	4705	6.5
3	3966	4.8	4161	5.3	4482	5.6	4708	6.2
4	3971	4.9	4165	5.4	4484	5.7	4708	6.2
5	3973	5.2	4165	5.4	4485	5.8	4709	6.4
6	3973	4.9	4167	5.2	4485	5.6	4710	6.5
7	3974	4.9	4167	5.5	4486	5.6	4711	6.5
8	3974	4.9	4169	5.2	4486	5.5	4712	6.4
9	3975	4.9	4169	5.3	4488	5.6	4712	6.5
10	3975	5.1	4259	5.3	4488	5.5	4713	6.0
11	3975	5.1	4261	5.1	4489	5.5	4713	6.5
12	3977	4.7	4262	4.9	4489	5.7	4714	6.5
13	3977	4.8	4263	5.5	4490	5.6	4714	6.0
14	3978	4.9	4263	5.5	4494	5.6	4715	6.2
15	3978	4.8	4263	5.4	4535	6.3	4716	6.5
16	3978	4.8	4264	5.4	4537	6.0	4716	6.4
17	3979	4.9	4264	5.5	4539	6.3	4717	6.5
18	3980	4.9	4264	5.5	4541	6.0	4719	6.6
19	3980	4.9	4264	5.3	4541	5.7	4719	6.5
20	3981	5.1	4264	5.3	4546	6.0	4720	6.0
21	3981	4.7	4265	5.4	4547	5.9	4720	6.4
22	3981	5.0	4265	5.2	4547	5.8	4721	6.5
23	3983	4.8	4265	5.2	4548	6.3	4723	6.0
24	3984	4.8	4266	5.5	4549	6.3	4724	5.9
25	3984	4.8	4266	5.6	4550	6.1	4725	6.2
26	4024	4.8	4266	5.4	4551	6.3	4726	6.0
27	4031	4.9	4266	5.5	4551	5.9	4728	6.0
28	4032	4.9	4267	5.6	4552	6.0	4729	6.0
29	4037	4.8	4267	5.8	4552	5.8	4731	6.1
30	4038	4.9	4267	5.4	4554	6.0	4732	6.4
31	4038	4.9	4269	5.2	4555	6.3	4732	6.5
32	4043	4.8	4270	5.7	4555	5.9	4734	6.0
33	4044	4.9	4271	5.6	4556	6.0	4735	6.2
34	4045	4.8	4271	5.5	4556	5.9	4862	6.6
35	4045	5.1	4271	5.2	4557	5.9	4864	6.8
36	4047	4.8	4274	5.3	4557	5.9	4866	6.6
37	4047	4.9	-	-	4558	6.0	4872	6.8
38	4048	5.0	-	-	4558	5.9	4873	6.6
39	4048	4.8	-	-	4559	6.0	4874	6.5

40	4048	4.7	-	-	4559	5.8	4875	6.7
41	4049	4.8	-	-	4559	5.6	-	-
42	4050	5.0	-	-	4561	5.9	-	-
43	4051	4.9	-	-	4561	5.7	-	-
44	4053	5.1	-	-	4561	5.8	-	-
45	4054	5.0	-	-	4561	5.9	-	-
46	4055	4.9	-	-	4562	6.2	-	-
47	4056	4.8	-	-	4562	5.9	-	-
48	4063	4.8	-	-	4562	5.9	-	-
49	-	-	-	-	4563	5.8	-	-
50	-	-	-	-	4563	6.0	-	-
51	-	-	-	-	4563	5.7	-	-
52	-	-	-	-	4564	6.0	-	-
53	-	-	-	-	4565	6.2	-	-
54	-	-	-	-	4565	6.0	-	-
55	-	-	-	-	4565	5.8	-	-
56	-	-	-	-	4565	5.9	-	-
57	-	-	-	-	4565	5.8	-	-
58	-	-	-	-	4565	6.0	-	-
59	-	-	-	-	4566	6.0	-	-
60	-	-	-	-	4566	6.0	-	-
61	-	-	-	-	4566	5.9	-	-
62	-	-	-	-	4566	5.7	-	-
63	-	-	-	-	4566	5.9	-	-
64	-	-	-	-	4567	5.8	-	-
65	-	-	-	-	4571	6.0	-	-
66	-	-	-	-	4572	5.8	-	-
67	-	-	-	-	4574	5.7	-	-
68	-	-	-	-	4580	5.9	-	-

#	4875 < rpm ≤ 5125	Power	5125 < rpm ≤ 5375	Power	5375 < rpm ≤ 5625	Power	5625 < rpm ≤ 5875	Power
1	4864	6.3	5126	7.3	5417	8.5	5680	9.4
2	4869	6.5	5127	7.2	5418	8.3	5681	9.3
3	4873	6.1	5127	7.2	5419	8.9	5682	9.7
4	4876	6.5	5176	7.5	5419	7.8	5682	9.3
5	4878	6.6	5177	7.4	5422	8.2	5685	9.4
6	4880	6.7	5179	7.5	5428	7.0	5689	9.5
7	4881	6.8	5180	7.5	5520	8.6	5687	9.2
8	4882	6.7	5180	7.0	5529	8.4	5691	9.5
9	4882	6.5	5181	7.3	5531	8.8	5698	9.3
10	4884	6.6	5182	7.4	5569	9.0	5699	9.5
11	4886	6.7	5184	7.4	5571	8.5	5676	9.1

12	4886	6.5	5185	7.1	5572	9.1	5679	9.5
13	4886	6.6	5185	7.4	5575	8.8	5682	8.5
14	4887	6.3	5187	7.4	5576	9.1	5681	11.0
15	4888	6.7	5232	7.8	5576	8.6	5680	7.9
16	4901	6.8	5233	7.6	5577	9.1	5679	8.5
17	4926	6.6	5236	7.6	5578	8.3	5683	8.0
18	4929	6.4	5236	7.9	5578	9.0	5684	8.9
19	4960	6.4	5237	7.7	5580	8.8	5685	9.3
20	4975	6.5	5237	7.8	5591	8.8	5686	9.5
21	4983	6.6	5238	7.6	5591	9.0	5692	10.1
22	4983	6.8	5238	7.9	5595	9.0	5690	9.7
23	4983	6.5	5239	7.6	5595	8.8	5691	9.1
24	4984	7.0	5240	7.7	5595	9.0	5695	8.5
25	4984	7.0	5242	7.6	5596	8.5	5696	8.5
26	4986	6.7	5247	7.8	5609	8.8	5699	9.6
27	4986	6.9	5248	7.7	5614	8.9	5701	9.1
28	4987	6.6	5248	7.6	5616	8.8	5703	9.3
29	4993	7.0	5249	7.7	-	-	5703	9.7
30	4993	6.8	5250	7.7	-	-	5768	10.4
31	4994	6.9	5251	7.6	-	-	5774	9.6
32	4998	6.8	5254	7.9	-	-	5789	10.0
33	4998	6.8	5254	8.2	-	-	5791	9.3
34	4999	6.7	5254	7.7	-	-	5795	9.1
35	5061	7.1	5254	7.6	-	-	5793	9.6
36	5062	6.8	5255	7.3	-	-	5796	10.0
37	5063	6.9	5256	7.8	-	-	5797	10.2
38	5066	6.8	5257	7.8	-	-	5801	9.3
39	5068	7.2	5257	7.7	-	-	5806	9.0
40	5070	7.1	5258	7.7	-	-	5810	8.5
41	5074	6.9	5258	7.3	-	-	5812	8.5
42	5079	7.0	5261	7.4	-	-	5811	10.5
43	5080	6.8	5262	7.8	-	-	5817	9.2
44	5085	7.1	5267	7.8	-	-	5815	8.7
45	5086	7.1	5268	7.6	-	-	5814	9.5
46	5088	6.9	5269	7.7	-	-	5821	8.5
47	5090	6.7	5269	7.6	-	-	5751	8.9
48	5091	7.1	5270	7.6	-	-	5753	9.7
49	5092	6.9	5273	7.5	-	-	5750	9.4
50	5096	7.1	5274	7.6	-	-	5749	9.1
51	5097	7.1	5275	8.1	-	-	5741	9.0
52	5099	7.0	5276	7.6	-	-	5746	9.0
53	5100	7.2	5276	7.9	-	-	5745	8.9

54	5101	7.0	5277	7.6	-	-	5754	9.5
55	5103	7.0	5279	7.7	-	-	5753	9.3
56	5107	7.3	5342	8.2	-	-	5747	9.1
57	5108	7.4	5343	8.0	-	-	5741	8.7
58	5108	7.1	5349	7.9	-	-	5740	9.4
59	5121	7.2	5351	7.8	-	-	5742	9.1
60	5122	7.2	5353	8.0	-	-	5741	9.1
61	5122	7.4	5354	8.2	-	-	5740	9.3
62	5123	7.2	5359	7.9	-	-	5737	9.1
63	5124	7.2	5361	7.9	-	-	5738	9.1
64	5124	7.3	5362	7.9	-	-	5736	8.9
65	-	-	-	-	-	-	5732	9.1

#	5875 < rpm ≤ 6125	Power	6125 < rpm ≤ 6375	Power	6375 < rpm ≤ 6625	Power
1	5890	9.3	6126	10.5	6419	11.1
2	5893	9.5	6128	10.3	6466	12.1
3	5923	9.6	6129	10.5	6472	11.4
4	5928	9.5	6130	10.3	6473	11.1
5	5929	9.6	6136	10.5	6479	11.5
6	5930	9.6	6140	10.1	6483	11.7
7	5931	9.9	6144	10.1	6500	11.5
8	5932	9.6	6151	10.0	6511	11.9
9	5933	10.1	6153	10.5	6521	11.4
10	5933	9.9	6156	10.4	6529	12.3
11	5935	9.7	6210	10.5	6532	11.7
12	5937	9.6	6210	10.2	6542	12.1
13	5937	9.5	6211	10.5	6543	11.6
14	5937	9.7	6212	10.5	-	-
15	5938	9.4	6215	11.5	-	-
16	5939	9.4	6216	10.8	-	-
17	5939	9.8	6218	11.3	-	-
18	5939	9.2	6218	11.5	-	-
19	5940	9.9	6218	10.4	-	-
20	5940	9.6	6219	10.9	-	-
21	5941	9.7	6219	11.5	-	-
22	5942	10.7	6219	10.5	-	-
23	5942	10.1	6222	10.3	-	-
24	6008	10.4	6223	11.0	-	-
25	6009	10.9	6225	11.1	-	-
26	6009	10.3	6225	11.0	-	-
27	6010	10.8	6226	9.2	-	-
28	6010	9.6	6226	10.7	-	-
29	6011	9.6	6227	10.9	-	-

30	6011	9.9	6229	10.9	-	-
31	6012	9.7	6229	10.7	-	-
32	6013	10.2	6230	11.3	-	-
33	6014	10.5	6230	11.7	-	-
34	6014	10.2	6230	11.8	-	-
35	6014	9.8	6230	10.9	-	-
36	6015	10.2	6230	10.5	-	-
37	6016	9.9	6230	10.3	-	-
38	6017	9.8	6231	11.3	-	-
39	6017	10.5	6232	12.7	-	-
40	6032	10.0	6233	11.2	-	-
41	6036	9.6	6233	11.3	-	-
42	6039	10.7	6233	10.6	-	-
43	6042	9.6	6234	12.4	-	-
44	6042	11.0	6237	10.1	-	-
45	6043	10.5	6240	10.8	-	-
46	6046	10.2	6242	11.3	-	-
47	6046	9.7	6243	10.2	-	-
48	6048	9.9	6244	11.2	-	-
49	6049	10.5	6246	10.2	-	-
50	6049	10.4	6263	10.7	-	-
51	6050	9.9	6266	11.2	-	-
52	6051	10.8	6274	10.8	-	-
53	6051	9.7	6277	10.2	-	-
54	6052	10.2	6278	11.0	-	-
55	6052	10.4	6280	11.8	-	-
56	6052	10.1	6285	10.7	-	-
57	6052	10.5	6290	11.2	-	-
58	6052	10.3	6291	11.2	-	-
59	6053	10.9	6293	10.7	-	-
60	6053	10.0	6294	11.0	-	-
61	6054	10.6	6295	10.7	-	-
62	6054	10.5	6297	11.1	-	-
63	6055	10.4	6297	11.9	-	-
64	6055	11.0	6298	11.2	-	-
65	6056	10.5	6362	11.2	-	-
66	6057	10.3	6367	10.7	-	-
67	6058	10.8	6367	10.7	-	-
68	6059	10.2	6368	11.5	-	-
69	6059	10.6	-	-	-	-
70	6059	10.4	-	-	-	-
71	6060	10.4	-	-	-	-

72	6062	10.5	-	-	-	-
73	6062	10.5	-	-	-	-
74	6065	10.6	-	-	-	-
75	6066	9.5	-	-	-	-
76	6070	10.8	-	-	-	-
77	6071	10.5	-	-	-	-
78	6073	9.9	-	-	-	-
79	6075	9.6	-	-	-	-
80	6080	9.8	-	-	-	-
81	6081	9.9	-	-	-	-
82	6083	10.8	-	-	-	-
83	6083	10.0	-	-	-	-
84	6084	9.8	-	-	-	-
85	6085	10.2	-	-	-	-
86	6087	10.2	-	-	-	-
87	6093	10.6	-	-	-	-
88	6096	10.2	-	-	-	-
89	6097	10.2	-	-	-	-
90	6097	10.2	-	-	-	-

## 11.8 Appendix 8: Determination of Power Efficiency

<b>Angular velocity (<math>\omega</math>)</b>	<b>Power Efficiency (<math>\eta</math>)</b>	<b>Fractional uncertainty (<math>\frac{\Delta\eta}{\eta}</math>)</b>	<b>Absolute uncertainty (<math>\Delta\eta</math>)</b>
<i>/rads<sup>-1</sup></i>	<i>kgm<sup>2</sup>s<sup>-3</sup></i>	-	<i>kgm<sup>2</sup>s<sup>-3</sup></i>
0	0	1.090	0
26	5.05041	1.492	7.53647
52	5.03806	1.497	7.54115
79	5.19595	1.501	7.79749
105	5.41957	1.504	8.15253
131	5.66842	1.508	8.54589
157	5.90947	1.511	8.92700
183	16.9106	1.582	26.7590
209	24.9627	1.622	40.4835
236	31.3804	1.651	51.8054
262	39.4344	1.685	66.4387
288	48.5075	1.722	83.5170
314	54.8055	1.748	95.8195
340	56.5343	1.760	99.5000
367	56.0104	1.765	98.8327
393	54.6171	1.766	96.4554
419	53.4560	1.767	94.4715
445	50.8639	1.764	89.7014
471	49.2979	1.763	86.8983
497	47.8633	1.761	84.2870
524	47.4140	1.762	83.5577
550	47.6857	1.765	84.1640
576	48.2416	1.769	85.3168
602	49.3993	1.774	87.6109
628	50.3016	1.777	89.4075
655	51.2764	1.782	91.3497
681	52.3214	1.786	93.4234
707	53.1726	1.789	95.1214

## 11.9 Appendix 9: Arduino Code for Modulating Motor RPM

```
int VoltPin = A0;
int SignalPin = 9;
int readVal;
float Volt;
#include <Servo.h>
Servo ESC;

void setup() {
  ESC.attach(9,1000,2000);
  Serial.begin(9600);
}
void loop() {
  readVal = analogRead(VoltPin);
  readVal = map(readVal, 0, 1023, 0, 180);
  ESC.write(readVal);
}
```